Computers in Biology and Medicine 111 (2019) 103329

Contents lists available at ScienceDirect

Computers in Biology and Medicine

journal homepage: www.elsevier.com/locate/compbiomed

Detecting connectivity in EEG: A comparative study of data-driven effective connectivity measures

Hanieh Bakhshayesh[a,b,*], Sean P. Fitzgibbon[c], Azin S. Janani[a,b], Tyler S. Grummett[a,b,d], Kenneth J. Pope[a,b]

[a] College of Science and Engineering, Flinders University, Adelaide, Australia
[b] Medical Device Research Institute, Flinders University, Adelaide, Australia
[c] Wellcome Centre for Integrative Neuroimaging, FMRIB, Nuffield Department of Clinical Neurosciences, University of Oxford, United Kingdom
[d] Centre for Neuroscience, College of Medicine and Public Health, Flinders University, Adelaide, Australia

ARTICLE INFO

Keywords:
Connectivity
EEG
Biomedical signal processing

ABSTRACT

In this paper, we perform the first comparison of a large variety of effective connectivity measures in detecting causal effects among observed interacting systems based on their statistical significance. Well-known measures estimating direction and strength of interdependence between time series are compared: information theoretic measures, model-based multivariate measures in the time and frequency domains, and phase-based measures. The performance of measures is tested on simulated data from three systems: three coupled Hénon maps; a multivariate autoregressive (MVAR) model with and without EEG as an exogenous input; and simulated EEG. No measure was consistently superior. Measures that model the data as MVAR perform well when the data are drawn from that model. Frequency domain measures perform well when the data have a clearly defined band of interest. When neither of these is true, information theoretic measures perform well. Overall, the measure with the best performance in a variety of situations and with a low computational cost is conditional Granger causality. Partial Granger causality and multivariate Granger causality are also good measures, but their computational cost rises rapidly with the number of channels. Copula Granger causality can also be used reliably, but its computational cost rises rapidly with the number of data.

1. Introduction

The identification of hidden dependencies among simultaneously observed time series from a complex dynamical system is an essential and challenging task in many scientific fields [1], and is of particular significance for brain dynamics. Representing patterns of interactions between different brain areas could be a major step to understanding the functional aspects of normal and pathological brain processes, such as the determination of the source of neuronal activity in epilepsy [2]. There has been wide-ranging research aimed at detecting underlying relationships (which may be nonlinear and/or nonstationary) in multi-output dynamic systems, to give useful insight into their spatio-temporal organisation [3]. One significant approach to defining dynamical links within a distributed system, such as the brain, is effective connectivity. Effective connectivity refers to the influence that one neural system has over another [4]. In the last few years, connectivity measures have become popular for the analysis of multiple electric signals recorded at the scalp in electroencephalograms (EEG). EEG has several clear advantages for studying the brain. Firstly, changes in the brain's electrical activity happen very quickly, and a very high time resolution (e.g. milliseconds or less) EEG system can capture these electrical events. Secondly, EEG electrodes are simply attached on the scalp. It is therefore a non-invasive procedure which allows relatively easy access to the human brain. Thirdly, in comparison to most other modalities, EEG equipment is relatively inexpensive and simple to use. Fourthly, EEG measures neuronal brain activity directly, not blood flow that is reacting to brain activity, i.e. it is a direct measurement not an indirect measurement. Hence our focus is on the modality of EEG.

The evaluation of connectivity measures on EEG presents several challenges. Human brains are complex nonstationary and nonlinear systems, and so EEG signals generated by the brain are typically nonlinear and nonstationary. Another big challenge in using EEG is the very small signal-to-noise ratio of the recordings, due to contamination of brain signals by a wide variety of noise sources. For example, muscle artefact is still a significant source of noise even after applying the best noise reduction techniques [5]. Therefore, it is extremely important

* Corresponding author. College of Science and Engineering, Flinders University, GPO Box 2100, Adelaide 5001, Australia.
E-mail address: hanieh.bakhshayesh@flinders.edu.au (H. Bakhshayesh).

https://doi.org/10.1016/j.compbiomed.2019.103329
Received 22 January 2019; Received in revised form 13 June 2019; Accepted 13 June 2019

Fig. 1. Two distinct connectivity patterns among three signals. A pairwise effective connectivity analysis may not distinguish these two patterns.

that a connectivity measure for EEG should be robust to noise, as well as be able to detect both nonlinear and nonstationary relationships between signals.

When there are more than two signals, which will always be the case for EEG, another significant challenge arises: the possibility of detecting "connections" that are not truly there. For example, the coupling scheme in Fig. 1 (left) may give the same pattern of connectivity as the scheme in Fig. 1 (right). Another example is where one signal drives both a second and third signal. Effective connectivity may incorrectly detect a causal influence from the second signal to the third signal, or vice versa. Ideally, we seek measures that are able to disambiguate these situations.

Some publications use real EEG for the comparison of measures [6]. The difficulty with using EEG is that we don't know when a measure is giving the "right" answer. We claim that there is merit in comparing measures on simulated data where the true connections are known, rather than on real EEG data where our understanding is imperfect.

Hence in this study, we focus on simulated systems that mimic EEG in some way, where we have some knowledge or control of the level of nonlinearity, nonstationary and noise, and where we know the true connectivity patterns.

There are several publications that compare many measures that include both functional (i.e. non-directed) measures and effective (i.e. directed) measures [6–8]. We argue that there are significant difficulties with comparing directed and nondirected measures. A comparison of functional measures has been published [9], so here we restrict the comparison to effective connectivity measures.

In addition, the literature generally takes a simplistic view that linear measures won't perform well on nonlinear datasets, but provides little evidence supporting this. It is therefore not sufficient to characterise the strength of the "linear component" in a nonlinear dataset, as a linear measure may not be totally insensitive to the "nonlinear component", and different measures may be differentially sensitive. Hence, we have chosen to test all measures on all datasets and let the results speak.

Previous studies of coupled identical and nonidentical systems mostly have focused on a few measures [3,10–15]. Many of the comparative studies of connectivity measures have focused on bivariate tests e.g. Ref. [16], while some studies have considered the effectiveness of only model-based measures, e.g. Refs. [2,17] or information theoretic measures, e.g. Refs. [18–20]. Hence, we claim that there is no thorough comparison of many measures on simulated data, and so we adopt this approach in this study.

Another significant issue is that different measures do not calculate values on the same scale. A higher value of connectivity in one measure may indicate no connection between two signals, whereas a lower value in a different measure may indicate a connection between the signals. Because they are not measuring on the same scale, significant variation in the raw values can be seen across measures. Hence to reliably compare different measures we need a statistical approach to identify when a connectivity value is significantly different from its background level.

To test the statistical significance of a connectivity value and determine whether connectivity is detected, we generate surrogates to give data with the same statistical properties as the simulated data but without the dependencies between signals. A collection of surrogate data can be analysed with the connectivity measure to obtain a distribution of connectivity values corresponding to signals without connectivity, and a threshold determined from the surrogate ensemble. If the connectivity measure calculated on the original data exceeds this threshold, then it is regarded as statistically significant.

In this study we consider a large variety of connectivity measures, comparing most well-known model-based multivariate measures and a phase-based measure. Where available, we used toolboxes to calculate the measures, otherwise we implemented measures according to the literature. Parameters of the measures, such as model order or number of bins, have been set according to standard approaches described in the literature. For the interested reader [21], have published a more detailed investigation into the effect of parameter selection. We applied all measures to linear and nonlinear synthetic data sets where we know the true relationship between the signals. First, we used a well-understood nonlinear system (three coupled Hénon maps), then an MVAR model with and without exogenous inputs, and finally we applied all measures to simulated EEG.

This paper is organised as follows. In section 2, we detail each studied effective connectivity measure, arranged by family, and review the use of surrogates for identifying significant connections. In section 3, we describe the simulated data and the statistical approach to identifying significant connectivity. In section 4, we apply the effective connectivity measures to the synthetic data and present the results. Finally, in section 5 we discuss the results and present our conclusions.

2. Effective connectivity measures

2.1. Granger causality and extended measures

Measures from the Granger causality family are popular choices for measuring causal connectivity in neuronal time series [22–25].

According to the classical Granger causality formulation, an autoregressive (AR) model is fitted to each of the time series separately. This model is then compared with a bivariate AR model, i.e. one where the past of both time series is included in the model. If the variance of the AR prediction error of the first time series is statistically significantly decreased by the inclusion of past measurements from the second time series, then the second time series is said to have a causal influence on the first one.

Now we give the mathematical formulation of Granger causality and then proceed to define conditional, partial and multivariate Granger causality. Let $x(t)$ and $y(t)$ be two stationary time series, then they can be represented by individual AR models

$$\begin{aligned} x(t) &= \sum_{\ell=1}^{p} A_{11\ell} x(t-\ell) + \eta_x(t) \\ y(t) &= \sum_{\ell=1}^{p} A_{22\ell} y(t-\ell) + \eta_y(t) \end{aligned} \tag{2-1}$$

where the noises $\eta_x(t)$, $\eta_y(t)$ are individually zero mean and uncorrelated with variances $\sum_1 = var(\eta_x(t))$ and $\sum_2 = var(\eta_y(t))$. Alternatively, they can be jointly represented by the following bivariate AR model

$$\begin{aligned} x(t) &= \sum_{\ell=1}^{p} A_{11\ell} x(t-\ell) + A_{12\ell} y(t-\ell) + e_x(t) \\ y(t) &= \sum_{j=1}^{p} A_{21\ell} x(t-\ell) + A_{22\ell} y(t-\ell) + e_y(t) \end{aligned} \tag{2-2}$$

where the noises $e_x(t)$ and $e_y(t)$ are individually zero mean and uncorrelated with variances $\sum_{xx} = var(e_x(t))$ and $\sum_{yy} = var(e_y(t))$ and covariance $\sum_{xy} = cov(e_x(t), e_y(t))$. The joint covariance matrix is therefore

$$\sum_{noise} = \begin{bmatrix} \sum_{xx} & \sum_{xy} \\ \sum_{yx} & \sum_{yy} \end{bmatrix} \tag{2–3}$$

The overall interdependence between two time series can be evaluated as:

$$F_{x,y} = ln\frac{\sum_1 \sum_2}{|\sum_{noise}|} \tag{2–4}$$

where $|\cdot|$ denotes the determinant of the enclosed matrix. $F_{x,y}$ is non-zero if the two time series are dependent i.e. the partial correlation between $x(t)$ and $y(t)$ (conditional on the past of those value) is non-zero. It is equal to the zero when the two time series are independent [26]. $F_{x,y}$ can be decomposed into three components

$$F_{x,y} = F_{y\to x} + F_{x\to y} + F_{x\cdot y} \tag{2–5}$$

where $F_{y\to x}$ is the measure of Granger causality from $y(t)$ to $x(t)$, given by

$$F_{y\to x} = \ln\frac{\sum_1}{\sum_{xx}} \tag{2–6}$$

and $F_{x\to y}$ is the measure of Granger causality from $x(t)$ to $y(t)$, given by

$$F_{x\to y} = \ln\frac{\sum_2}{\sum_{yy}} \tag{2–7}$$

and $F_{x\cdot y}$ is a measure of the instantaneous causality, given by

$$F_{x\cdot y} = ln\frac{\sum_{xx}\sum_{yy}}{|\sum_{noise}|}$$

These three quantities are all zero when the two time series are independent, and can be non-zero if and only if they are dependent. In practice, classical Granger causality is rarely used in EEG where there are many time series. Instead, an extension of Granger causality that can differentiate between direct and cascade influences is usually chosen. We also note that some implementations of Granger causality can exhibit statistical bias; see Ref. [27] for a discussion. Here we have used the MVGC toolbox for all GC measures to avoid these issues [28].

2.1.1. Time domain conditional Granger causality

Conditional Granger causality (CGC) is the simplest extension, and incorporates knowledge of a third time series. Specifically, CGC estimates the influence of one signal on another given knowledge of a third [16,29,30]. Let $W(t) = [\omega_1(t), \omega_2(t), ..., \omega_n(t)]^T$ be a set of n stationary time series, where T indicates matrix transposition. Suppose that $W(t)$ has been decomposed into three non-overlapping sets of time series $x(t)$, $y(t)$ and $z(t)$ with dimensions k, l and m respectively, where $m + l + k = n$. The conditional Granger causality from $y(t)$ to $x(t)$ given $z(t)$ is defined as:

$$F_{y\to x|z} = \ln\frac{var(x(t)|x(t-1), x(t-2), \cdots, z(t-1), z(t-2)\cdots)}{var(x(t)|x(t-1), x(t-2)\cdots y(t-1)y(t-2), \cdots, z(t-1)z(t-2), \cdots)} \tag{2–8}$$

The above time domain definition can be achieved by combining two AR models. First $x(t)$ and $z(t)$ are supposed to be related by the following bivariate model.

$$\begin{aligned} x(t) &= \sum_{\ell=1}^{P} D_{11_\ell} x(t-\ell) + D_{13_\ell} z(t-\ell) + \Theta(t) \\ z(t) &= \sum_{\ell=1}^{P} D_{31_\ell} x(t-\ell) + D_{33_\ell} z(t-\ell) + \Psi(t) \end{aligned} \tag{2–9}$$

where the noises $\Theta(t)$ and $\Psi(t)$ are zero mean and uncorrelated over time.

Let $cov(\Theta(t), \Psi(t)) = \sum_{\psi\Theta}$ then the noise covariance matrix for the bivariate model can be presented as

$$\sum_{noise(1)} = \begin{bmatrix} \sum_{\Theta\Theta} & \sum_{\Theta\psi} \\ \sum_{\psi\Theta} & \sum_{\psi\psi} \end{bmatrix} \tag{2–10}$$

The second AR model is the following trivariate model involving $x(t)$, $y(t)$ and $z(t)$

$$\begin{aligned} x(t) &= \sum_{\ell=1}^{P} B_{11_\ell} x(t-\ell) + B_{12_\ell} y(t-\ell) + B_{13_\ell} z(t-\ell) + e_x(t) \\ y(t) &= \sum_{\ell=1}^{P} B_{21_\ell} x(t-\ell) + B_{22_\ell} y(t-\ell) + B_{23_\ell} \\ &\quad z(t-\ell) + e_y(t) \\ z(t) &= \sum_{\ell=1}^{P} B_{31_\ell} x(t-\ell) + B_{32_\ell} y(t-\ell) + B_{33_\ell} \\ &\quad z(t-\ell) + e_z(t) \end{aligned} \tag{2–11}$$

where the noises $e_x(t)$, $e_y(t)$ and $e_z(t)$ are again supposed to be zero mean and uncorrelated over time.

Let $cov(e_x(t), e_y(t)) = \sum_{xy}$ then the covariance of all the noises is given by:

$$\sum_{noise(2)} = \begin{bmatrix} \sum_{xx} & \sum_{xy} & \sum_{xz} \\ \sum_{yx} & \sum_{yy} & \sum_{yz} \\ \sum_{zx} & \sum_{zy} & \sum_{zz} \end{bmatrix} \tag{2–12}$$

The conditional Granger causality from $y(t)$ to $x(t)$ given $z(t)$ is defined as:

$$F_{y\to x|z} = \ln\frac{|\sum_{\Theta\Theta}|}{|\sum_{xx}|} \tag{2–13}$$

If the inclusion of $y(t)$ results in improved prediction of $x(t)$ ($y(t)$ has a direct influence on $x(t)$), $|\sum_{\Theta\Theta}| > |\sum_{xx}|$ and $F_{y\to x|z} > 0$. In contrast if $x(t)$ and $y(t)$ are independent, $|\sum_{\Theta\Theta}| = |\sum_{xx}|$ and $F_{y\to x|z} = 0$ [31].

2.1.2. Conditional frequency domain Granger causality

The time-domain conditional Granger causality can be transformed to the spectral domain. First, we normalise both the bivariate and trivariate models in equations (2-9) and (2-11). Normalisation will remove the correlation between noises in bivariate and noises in trivariate models and ensure that the causality is the result of the interactions between the regression terms in trivariate model only.

For normalisation both equation of the bivariate model are pre-multiplied by the following transformation matrix

$$q = \begin{bmatrix} q_{11} & q_{12} \\ q_{21} & q_{22} \end{bmatrix} \tag{2–14}$$

where $q_{11} = I_m$, $q_{12} = 0$, $q_{21} = \sum_{\psi\Theta} \sum_{\psi\psi}^{-1}$ and $q_{22} = I_k$ and both side of the trivariate model are pre-multiplied by

$$p_1 = \begin{bmatrix} p_{11} & p_{12} & p_{13} \\ p_{21} & p_{22} & p_{23} \\ p_{31} & p_{32} & p_{33} \end{bmatrix} \tag{2–15}$$

where $p_{11} = I_m$, $p_{12} = 0$, $p_{13} = 0$, $p_{21} = -\sum_{yx}\sum_{xx}^{-1}$, $p_{22} = I_n$, $p_{23} = 0$,

$$p_{31} = \left(\sum_{zy} - \sum_{zx}\sum_{xx}^{-1}\sum_{xy}\right)\left(\sum_{yy} - \sum_{yx}\sum_{xx}^{-1}\sum_{xy}\right)^{-1}\left(\sum_{yx}\sum_{xx}^{-1}\right) - \sum_{zx}\sum_{xx}^{-1},$$

$$p_{32} = -\left(\sum_{zy} - \sum_{zx}\sum_{xx}^{-1}\sum_{xy}\right)\left(\sum_{yy} - \sum_{yx}\sum_{xx}^{-1}\sum_{xy}\right)^{-1} \text{ and } p_{33} = I_k$$

The time domain conditional Granger causality can be expressed in the frequency domain as [30].

$$F_{y\to x|z}(f) = \ln\frac{|\sum_{\Theta}|}{|Q_{xx}(f)\sum_{xx}Q_{xx}^{*}(f)|} \tag{2–16}$$

where

$$Q(f) = \begin{bmatrix} Q_{xx}(f) & Q_{xy}(f) & Q_{xz}(f) \\ Q_{yx}(f) & Q_{yy}(f) & Q_{yz}(f) \\ Q_{zx}(f) & Q_{zy}(f) & Q_{zz}(f) \end{bmatrix}$$

$$= \begin{bmatrix} G_{xx}(f) & 0 & G_{xz}(f) \\ 0 & 1 & 0 \\ G_{zx}(f) & 0 & G_{zz}(f) \end{bmatrix}^{-1} \begin{bmatrix} H_{xx}(f) & H_{xy}(f) & H_{xz}(f) \\ H_{yx}(f) & H_{yy}(f) & H_{yz}(f) \\ H_{zx}(f) & H_{zy}(f) & H_{zz}(f) \end{bmatrix}$$

and $|\sum_{\Theta}| = Q_{xx}(f)\sum_{xx} Q^{*}_{xx}(f) + Q_{xy}(f)\sum_{yy} Q^{*}_{xy}(f) + Q_{xz}(f)\sum_{zz} Q^{*}_{xz}(f)$

The quantities in the above expression come from $G(f)$ and $H(f)$ which are the transfer function matrices for the normalised bivariate and trivariate models respectively.

2.1.3. Partial Granger causality

The ability of the conditional Granger causality to measure causal influence of one signal on another signal and deal with indirect interactions seriously depends on the all relevant variable in the system. Often it is impossible to measure all variables involved in the system due to the existence of the both exogenous and latent inputs. Thus, dealing with these unmeasured variables is the critical challenge when conditional Granger causality is applied to the signals in the real world. To confront this problem, the partial Granger causality has been proposed [32].

The partial Granger causality between $x(t)$ and $y(t)$ by removing all the effects of $z(t)$, can be evaluated by partitioning the noise covariance matrix $\sum_{noise(1)}$ (introduced in equations (2–10))

$$\sum_{noise(1)} = \left[\begin{array}{c|c} \sum_{\Theta\Theta} & \sum_{\Theta\Psi} \\ \hline \sum_{\Psi\Theta} & \sum_{\Psi\Psi} \end{array}\right] = \begin{bmatrix} \sum_{\Theta\Theta} & \sum_{\Theta\Psi} \\ \sum_{\Psi\Theta} & \sum_{\Psi\Psi} \end{bmatrix} \tag{2–17}$$

Hence the variance of Θ by eliminating the influence of Ψ can be defined as:

$$cov(\Theta, \Theta) - cov(\Theta, \Psi)cov(\Psi, \Psi)^{-1}cov(\Psi, \Theta) = \sum_{\Theta\Theta} - \sum_{\Theta\Psi}\sum_{\Psi\Psi}^{-1}\sum_{\Psi\Theta} \tag{2–18}$$

Similarly, we can partition $\sum_{noise(2)}$

$$\sum_{noise(2)} = \left[\begin{array}{c|c} \sum_{xx} & \sum_{xz} \\ \hline \sum_{zx} & \sum_{zz} \end{array}\right] \tag{2–19}$$

Similarly, the variance of the $e_x(t)$ by eliminating the influence the $e_z(t)$ is given by

$$cov(e_x(t), e_x(t)) - cov(e_x(t), e_z(t))cov(e_z(t), e_z(t))^{-1}cov(e_z(t), e_x(t)) = \sum_{xx} - \sum_{xz}\sum_{zz}^{-1}\sum_{zx} \tag{2–20}$$

Hence the measure for partial Granger causality from $y(t)$ to $x(t)$ by eliminating the effect of $z(t)$ can be expressed as

$$F_{y\to x|z} = \ln\left(\frac{\sum_{\Theta\Theta} - \sum_{\Theta\Psi}\sum_{\Psi\Psi}^{-1}\sum_{\Psi\Theta}}{\sum_{xx} - \sum_{xz}\sum_{zz}^{-1}\sum_{zx}}\right) \tag{2–21}$$

2.1.4. Copula-based Granger causality

Let we have a set of time series $x_1(t)$, ...,$x_n(t)$. First the marginal distribution of each time series, $\tilde{F}_i$ are estimated. Next the observations are mapped to the Gaussian copula domain as $\tilde{f}_i(x_i(t)) = \tilde{\mu}_i + \tilde{\sigma}_i\Phi^{-1}(\tilde{F}_i(x_i(t)))$, where μ and σ are the mean and variance and $\Phi(\cdot)$ is the cdf of the unit Gaussian distribution. Finally, the Granger causality among the $\tilde{f}_i(x_i(t))$ is estimated [33].

Based on the copula method, the marginal properties of the data are separated from its dependency structure. But the interdependence between the mapped time series in the copula space are the same as the interdependence between the original time series. Bahadori and Liu in Ref. [33] showed that copula-based Granger causality is consistent in high dimensions, unlike Granger causality, and that it is able to efficiently capture non-linearity in the data. For our calculations, we used a toolbox based on [34].

2.1.5. Multivariate Granger causality

So far, we have considered pairwise Granger causality and its extensions (CGC and PGC), which consider at most three time series at a time. They can be applied to more time series, but this is done by repeated application to all sets of two or three time series as appropriate. In this section we define multivariate Granger causality, which analyses all signals simultaneously to determine direct and indirect connections involving more than three signals.

Let $x(t) = [x_1(t), x_2(t), ...x_n(t)]$ be an n-dimensional multivariate stochastic process. The influence of the time series $x_j(t)$ on $x_i(t)$ can be calculated as:

$$F_{xj(t)\to x_i(t)} = \frac{\sum_{x_i(t)|x_1(t),\cdots x_{j-1}(t)x_{j+1}(t),\cdots x_n(t)}}{\sum_{x_i(t)|x_1(t)\cdots x_n(t)}} \tag{2–22}$$

This is similar to conditional Granger causality, but we are conditioning on all other time series, not simply one time series.

2.1.6. Multivariate frequency domain Granger causality

The calculation of the multivariate Granger causality can also be performed in the spectral domain. The MVAR model of a set of n signals $x_1(t)$, $x_2(t)$,..., $x_n(t)$ is given by Ref. [35]:

$$\begin{bmatrix} x_1(t) \\ \vdots \\ x_n(t) \end{bmatrix} = \sum_{l=1}^{P} A_l \begin{bmatrix} x_1(t-l) \\ \vdots \\ x_n(t-l) \end{bmatrix} + \begin{bmatrix} e_1(t) \\ \vdots \\ e_n(t) \end{bmatrix} \tag{2–23}$$

where P is the model order, the model coefficients A_i are $n \times n$ matrices, and each $e_i(t)$ is a zero-mean Gaussian random process. According to this model, each signal is assumed to linearly dependent on its own p past values and the p past values of the other signals, plus an innovation or noise input. Transforming to the frequency domain gives $X(f)[I - A(f)] = E(f)$, where $A(f) = \sum_{l=1}^{P} A_l e^{2\pi i f l}$, and hence the covariance matrix $S(f)$ of the model signals is $S(f) = H(f)VH(f)^H$, where $H(f) = [I - A(f)]^{-1}$ and V is the prediction error covariance matrix [35].

The calculation of the multivariate Granger causality can also be performed in the spectral domain using a factorisation theorem that specifies that any given spectral density matrix $S(f)$ can be decomposed into a set of unique minimum-phase functions $\psi(f)$ [36,37].

$$S(f) = \psi(f)\psi^H(f) \tag{2–24}$$

Using a Fourier-like analysis on the minimum-phase functions, we can calculate the noise covariance matrix $\sum$ and minimum phase-transfer function $H(f)$ as

$$\psi(f) = \sum_{k=0}^{\infty} R_k e^{ik2\pi f} \qquad \sum = R_0 R_0^T \qquad H(f) = \psi(f)R_0^{-1} \tag{2–25}$$

where T stands for matrix transposition.

As discussed in section 2.1 after fitting the MVAR model to the time series and Fourier transforming, the overall spectral density matrix can be calculated as

$$S(f) = H(f)\sum H^H(f)$$

where H denotes Hermitian transpose and $\sum$ is the covariance matrix of the noise vector.

The conditional Granger causality needs to compare this estimate of the noise covariance with noise covariance from a model that excludes

the jth time series. We obtain this by taking the overall spectral density matrix $S(f)$ and removing the jth row and columns. The reduced spectral density matrix $\bar{S}(f)$ can now be factorised:

$$\bar{S}(f) = G(f) \overline{\sum} G^H(f) \tag{2–26}$$

where $G(f)$ is the transfer function matrix and $\overline{\sum}$ is the noise covariance matrix for the selected subsystem. To calculate the normalisation matrix $Q(f)$, we need to extend the transfer function matrix $G(f)$ by inserting zeros for the jth row and column, but with 1 at their intersection:

$$Q(f) = \begin{bmatrix} G_{(1\ldots j-1)(1\ldots j-1)}(f) & 0 & G_{(1\ldots j-1)(1\ldots j-1)}(f) \\ 0\ldots 0 & 1 & 0\ldots 0 \\ G_{(j+1\ldots n)(1\ldots j-1)}(f) & 0 & G_{(j+1\ldots n)(j+1\ldots n)}(f) \end{bmatrix}^{-1} H(f) \tag{2–27}$$

Finally, we can use equations (2–17) and calculate the conditional Granger causality from the jth time series to the ith time series as:

$$F_{j\to i}(f) = \ln \frac{|\bar{\Sigma}_{ii}|}{|Q_{ii}(f) \sum_{ii} Q_{ii}^*(f)|} \tag{2–28}$$

2.2. Directional measures based on coherence

It is useful to define the inverse of the spectral density matrix and decompose it as

$$P(f) = S^{-1}(f) = \bar{A}^H(f) \sum^{-1} \bar{A}(f) \tag{2–29}$$

The ijth element of $S(f)$ and $P(f)$ can be represented as

$$S_{ij}(f) = h_i(f) \sum h_j^H, \quad P_{ij}(f) = \bar{a}_i^H(f) \sum^{-1} \bar{a}_j(f) \tag{2–30}$$

where $h_m(f)$ and $\bar{a}_m$ are the mth rows of the transfer function matrix $H(f) = [h_1(f), \cdots h_n(f)]^T$ and coefficient matrix $\bar{A}(f) = [\bar{a}_1(f), \cdots \bar{a}_n(f)]^T$. Since the input white noises are uncorrelated even at lag zero, their covariance matrix $cov(e(t))$ reduces to diagonal form as

$$\sum = diag(\sigma_k{}^2)$$

and its inverse to diagonal matrix

$$\sum^{-1} = diag\left(\frac{1}{\sigma_k{}^2}\right)$$

where $\sigma_k{}^2$ is the variance of $e_k(t)$. $S_{ij}(f)$ and $P_{ij}(f)$ can be factorised into:

$$S_{ij}(f) = \sum_{m=1}^{n} \sigma_m{}^2 H_{im}(f) H_{jm}(f) \tag{2–31}$$

$$P_{ij}(f) = \sum_{m=1}^{n} \frac{1}{\sigma_m{}^2} \bar{A}^H{}_{im}(f) \bar{A}_{jm}(f) \tag{2–32}$$

All coherence family measures were calculated using the Extended Multivariate Autoregressive Modelling Toolbox [38].

2.2.1. Directed coherence

In order to define directed coherence (DC) first we need to introduce coherence. The coherence function $c(f)$is the square of the cross spectrum, normalised by the auto-spectra of the two signals [39]:

$$c(f) = \frac{|(C_{xy}(f))|^2}{|(C_{xx}(f))||(C_{yy}(f))|} \tag{2–33}$$

where $(\cdot)$ stands for average over the segments and $C_{xy}(f)$ is the linear correlations in frequency domain which can be computed by means of the cross spectrum:

$$C_{xy}(f) = E[X(f)Y^*(f)] \tag{2–34}$$

where $E[.]$ is the expectation operator, $X(f)$ is the (discrete) Fourier transform of $x(n)$, the asterisk indicates complex conjugation, and f is frequency. In practice, a finite number of samples will give a noisy estimate of (cross- and auto-) spectra. To reduce the noise, signals are segmented into equal length pieces, and the spectra of each segment is averaged (Welch's method [40]).

By substituting for $S_{ij}(f)$ from equations (2–30) in the coherence equation, the following directional coherence can be obtained

$$c_{ij}(f) = \frac{h_i(f) \sum h_j^H(f)}{\sqrt{h_i(f) \sum h_i^H(f)} \sqrt{h_j(f) \sum h_j^H(f)}} = \sum_{m=1}^{n} \frac{\sigma_m H_{im}(f)}{\sqrt{S_{ii}(f)}} \frac{\sigma_m H^H{}_{jm}(f)}{\sqrt{S_{jj}(f)}} = \sum_{m=1}^{n} \gamma_{im} \gamma_{jm}^* \tag{2–35}$$

The term γ_{ij} in the above equation measures the influence of x_j on x_i, the so-called directed coherence DC [35].

$$\gamma_{ij}(f) = \frac{\sigma_j H_{ij}(f)}{\sqrt{S_{ii}(f)}} \tag{2–36}$$

where $S_{ii}(f) = \sum_{m=1}^{n} \sigma_m^2 |H_{im}(f)|^2$

DC can be normalised as $|\gamma_{ij}(f)|^2$, which gives 0 in the absence of any directed influence from x_j on x_i at the frequency f, and achieves 1 in the presence of maximum influence.

2.2.2. Directed transfer function

Directed transfer function (DTF) also uses the transfer function matrix $H(f)$, but normalises it in a simpler way [41]:

$$DTF_{ij} = \frac{H_{ij}(f)}{\sqrt{\sum_{m=1}^{n} |H_{im}(f)|^2}} \tag{2–37}$$

DTF can be considered as a particular case of DC in which all input variances are 1 ($\sigma_1^2 = \sigma_2^2 = \ldots \sigma_n^2 = 1$).

2.2.3. Partial directed coherence and generalised partial directed coherence

In order to define partial directed coherence, first we need to introduce partial coherence (PC). The partial coherence between a pair of signals involves the use of a MVAR model. As discussed in section 2.1.6 after fitting the MVAR model to the time series and Fourier transforming, the overall spectral density matrix can be calculated as

$$S(f) = H(f) \sum H^H(f)$$

Then the partial coherence between $x_i(t)$ and $x_j(t)$ is defined using $M_{ij}(f)$, the $(i,\ j)^{\text{th}}$ minor of $S(f)$, as [35,42]:

$$C_{ij}(f) = \frac{M_{ij}(f)}{\sqrt{M_{ii}(f)} \sqrt{M_{jj}(f)}} \tag{2–38}$$

The partial coherence $C_{ij}(f)$ estimates the coherence of a pair signals $x_i(t)$ and $x_j(t)$ at each frequency f with the influence of other signals statistically eliminated.

In the complex network where there are both direct and indirect pathways between two time series, both DC and DTF represent a balance of signal power that spreads from one time series to another via any of these pathways. In other words, a non-zero DC from time series x_j to x_i can be the result of either indirect or direct influence. To confront these issues, the measure partial coherence has been proposed.

We can substitute for $P_{ij}(f)$ from equations (2–32) into the expression for partial coherence in equation (2–38), and write:

$$\Pi_{ij}(f) = \frac{\bar{a}_i^H(f) \sum^{-1} \bar{a}_j(f)}{\sqrt{\bar{a}_j^H(f) \sum^{-1} \bar{a}_j(f)} \sqrt{\bar{a}_i^H(f) \sum^{-1} \bar{a}_i(f)}} = \sum_{m=1}^{n} \frac{\frac{1}{\sigma_m} \bar{A}_{mj}(f)}{\sqrt{P_{jj}(f)}} \frac{\frac{1}{\sigma_m} \bar{A}_{mi}^H(f)}{\sqrt{P_{ii}(f)}} = \sum_{m=1}^{n} \pi_{im} \pi_{jm}^H \tag{2–39}$$

The term π_{ij} in equation (2–39) measures the influence of x_j on x_i, namely generalised partial directional coherency (GPDC) [43].

$$\pi_{ij} = \frac{\frac{1}{\sigma_m}\bar{A}_{ij}(f)}{\sqrt{P_{jj}(f)}} \tag{2–40}$$

where $\sqrt{P_{jj}(f)} = \sqrt{\sum_{m=1}^{n} \frac{1}{(\sigma_m)^2} |\bar{A}_{jm}(f)|^2}$

The original version of equations (2–39) introduced in Ref. [35] did not include the input noise variance and was named partial directed coherence (PDC). The PDC is thus given by:

$$\pi_{ij}^{\omega} = \frac{\bar{A}_{ij}(f)}{\sqrt{\sum_{m=1}^{n} |\bar{A}_{mj}(f)|^2}} \tag{2–41}$$

2.2.4. Direct directed transfer function

To distinguish between direct causal connections between two signals and connections which are mediated by another signal, the directed directed transfer function (DDTF) was introduced [44]. It is defined by multiplying the directed transfer function by the partial coherence. The DDTF from signal j to signal i is defined as:

$$DDTF_{ij} = \pi_{ij}^{\omega}\, DTF_{ij} \tag{2–42}$$

2.2.5. Extended directed coherence and extended partial directed coherence

The MVAR model introduced in equation (2–23) uses lagged versions of the time series in the regression model. In other word this model describes the effect of the past of one time series on another, but it does not account for instantaneous (not lagged) effects among time series.

Faes and Nollo proposed in Ref. [45] an alternative MVAR model that includes instantaneous effects into the model of the time series. Consider the following extended MVAR model with 0 lag inclusion

$$x(t) = \sum_{\ell=0}^{P} B(\ell)x(t-\ell) + u(t) \tag{2–43}$$

where $u(t) = [u_1(t), u_2(t), \cdots, u_m(t)]^T$ is a vector of zero-mean uncorrelated white noise processes with diagonal covariance matrix $\hat{\sum} = diag(\hat{\sigma}_k{}^2)$, and the diagonal of $B(0)$ is constrained to be zero.

We can rewrite equation (2–43) as

$$x(t) = B(0)x(t) + \sum_{\ell=1}^{P} B(\ell)x(t-\ell) + u(t)$$

To find the relationship between the above extended MVAR model and the classic MVAR model in equations (2–23), the term $B(0)x(t)$ is moved to the left

$$x(t)[I - B(0)] = \sum_{\ell=1}^{P} B(\ell)x(t-\ell) + u(t)$$

Substituting for $x(t)$ in this equation with $x(t)$ from original MVAR models yields:

$$\sum_{j=1}^{P} A(\ell)x(t-\ell) + e(t)[I - B(0)] = \sum_{\ell=1}^{P} B(\ell)x(t-\ell) + u(t)$$

Therefore $B(\ell) = LA(\ell)$ and $u(t) = Le(t)$ where $L = [I - B(0)]^{-1}$ and $\sum = L\hat{\sum} L^T$

Hence the following algorithm can be used for forming the extended MVAR model to describe causal interactions among time series including instantaneous influence.

1. The noise covariance matrix $\sum$ and $A(\ell)$ for the classic MVAR model are calculated.
2. The noise covariance matrix $\sum$ is decomposed to yield the diagonal noise covariance matrix $\hat{\sum}$ and the lower triangular matrix L.
3. The instantaneous effects matrix $B(0)$ and coefficient matrices $B(\ell)$ can be calculated using above outlined relationships.

In the spectral domain we can represent the extended MVAR model by the Fourier transform of equations (2–43) as

$$X(f) = B(f)X(f) + U(f) \tag{2–44}$$

where $B(f)$ is the coefficient matrix in frequency domain

$$B(f) = B(0) + \sum_{\ell=1}^{P} B(\ell)e^{-i2\pi f \ell T}$$

The spectral matrix $S(f)$ and its inverse $P(f)$ of the extended MVAR model can be expressed as:

$$S(f) = G(f)\hat{\sum} G^H(f)\,,\; P(f) = \bar{B}^H(f)\hat{\sum}^{-1}\bar{B}(f) \tag{2–45}$$

where the transfer function $G(f) = [I - B(f)]^{-1}$.

Following the procedure described for GDC and GPDC, we can define the extended directional coherence (EDC) ξ_{ij} and extended partial directed coherence (EPDC) χ_{ij} from x_j to x_i as [46]:

$$\xi_{ij}(f) = \frac{\hat{\sigma}_j G_{ij}(f)}{\sqrt{\sum_{m=1}^{n} \hat{\sigma}_m^2 |G_{im}(f)|^2}} \tag{2–46}$$

$$\chi_{ij} = \frac{\frac{1}{\hat{\sigma}_j}\bar{B}_{ij}(f)}{\sqrt{\sum_{m=1}^{n} \frac{1}{(\hat{\sigma}_m)^2} |\bar{B}_{mj}(f)|^2}} \tag{2–47}$$

2.3. Information-theoretic measures

The information-theoretic measures analyse information flow between two systems or between constituent subsystems of a complex system. These methods do not explicitly model the underlying interaction, and hence do not make any assumption about the underlying system [47,48].

In this section, we provide a detailed overview of two groups of information-theoretic approaches for measuring interdependencies between signals: similarity measures, based on mutual information; and dissimilarity measures, that quantify the information divergence between two signals. As these measures estimate a dissimilarity, their minimum corresponds to maximum similarity. Hence, following [49], we have normalised and inverted these measures so that zero corresponds to no synchrony and one corresponds to maximum synchrony.

We first introduce the concept of entropy which measures the uncertainty of a discrete random variable. Let X and Y be random variables with probability density functions $\rho(x) = \Pr\{X = x\}$ and $\rho(y) = \Pr\{Y = y\}$, then the Shannon entropy $H(X)$ measures the average amount of information gained from an observation of X. It is defined as:

$$H(X) = -\sum_{x} \rho(x)\log(\rho(x)) \tag{2–48}$$

Similarly, the joint entropy $H(X, Y)$ is:

$$H(X, Y) = -\sum_{x}\sum_{y} \rho(x, y)\log(\rho(x, y)) \tag{2–49}$$

where $\rho(x, y) = P_r\{X = x, Y = y\}$ is the joint probability of these values occurring together.

Finally, the conditional entropy $H(X|Y)$ of X given Y is defined using the conditional probability $\rho(x|y) = P_r\{X = x|Y = y\}$ as:

$$H(X|Y) = -\sum_{x}\sum_{y} \rho(x, y)\log(\rho(x|y)) \tag{2–50}$$

The joint entropy can be expressed in terms of the conditional entropy and the Shannon entropy as $H(X, Y) = H(X|Y) + H(Y)$. Mutual information $I(X; Y)$ quantifies the amount of shared information between X and Y [50]:

$$I(X;Y) = \sum_x \sum_y \rho(x,y)\log\left(\frac{\rho(x,y)}{\rho(x)\rho(y)}\right) \tag{2–51}$$

Mutual information can be equivalently expressed as

$$I(X;Y) = H(X) - H(X|Y) = H(Y) - H(Y|X) = H(X) + H(Y) - H(X,Y) = H(X,Y) - H(X|Y) - H(Y|X) \tag{2–52}$$

Mutual information is not normalised, so to use it as a measure of synchronisation we need to normalise it. Several normalisations have been proposed, including NMI_L by Lancichinetti et al. [51] in:

$$NMI_L = 1 - \frac{1}{2}\left(\frac{H(X|Y)}{H(X)} + \frac{H(Y|X)}{H(Y)}\right) \tag{2–53}$$

and the normalised mutual information NMI_{FJ} by Fred and Jain in Ref. [52]:

$$NMI_{FJ} = \frac{2I(X;Y)}{H(X) + H(Y)} \tag{2–54}$$

Following [53], NMI_L is less numerically stable, so in this paper we use NMI_{FJ}.

In the following, we define information theoretic measures which allows to detect causal relationship between time series.

2.3.1. Transfer entropy

Mutual information is a symmetric measure that describes shared information and not causal relationships. To obtain a causal measure within the information theoretic framework, transfer entropy (TE) has been proposed [54].

TE can be defined in terms of conditional mutual information [54–56], we can say that random variable X cause Y if the uncertainty about Y is decreased by the past knowledge of X.

The conditional mutual information $I(X;Y|Z)$ of the random variables A and B given the variable Z is defined as [57].

$$I(X;Y|Z) = H(X|Z) + H(Y|Z) - H(X,Y|Z) \tag{2–55}$$

where $H(X|Z)$ is the conditional entropy of X given Z, as defined in equation (2–50).

The transfer entropy from X to Y then corresponds to the conditional mutual information $I(Y_t; X_{t-1:t-\ell}|Y_{t-1:t-\ell})$, which quantifies the information about the current state of the response system, Y_t, obtained from the past of the driving system, $X_{t-1:t-\ell}$, that is not already contained in the past of the response system $Y_{t-1:t-\ell}$. Thus TE in terms of entropy is given by

$$TE_{X\to Y} = H(Y_t|Y_{t-1:t-\ell}) + H(X_{t-1:t-\ell}|Y_{t-1:t-\ell}) - H(Y_t, X_{t-1:t-\ell}|Y_{t-1:t-\ell}) \tag{2–57}$$

Since $H(X|Y) = H(X,Y) - H(Y)$, where $H(X,Y)$ denotes the joint entropy is outlined in equation (2–49), the preceding expressions can be also written in the following form:

$$TE_{X\to Y} = H(Y_t, Y_{t-1:t-\ell}) - H(Y_{t-1:t-\ell}) + H(X_{t-1:t-\ell}, Y_{t-1:t-\ell}) - H(Y_t, X_{t-1:t-\ell}, X_{t-1:t-\ell}) \tag{2–58}$$

There are several algorithms for calculating TE [58–64], but while they may be more accurate or have less bias, they are typically much slower at calculating the required three-dimensional entropy. In this study, we used the binning method. The method is based on the discretisation of the time series into Q equiquantal bins, i.e. bins with equal counts and therefore different widths. Conditional mutual information can then be calculated by a simple box-counting algorithm based on equiquantal marginal bin [65]. Transfer entropy calculations used the INTERACT toolbox, and partial measures used the TIM toolbox [66].

2.3.2. Partial transfer entropy

In the previous sections, we described transfer entropy as a causality measure in terms of the entropy between two time series, ignoring all other time series. If two time series are a part of a bigger interacting system, e.g. three interacting time series X, Y and Z, then transfer entropy will estimate not only direct interactions between them, but also estimate indirect interactions including a third time series. To estimate only the information transferred directly between the two time series, we need to take into account the influence of the third time series. Partial transfer entropy (PTE) is the extension of TE designed for measuring the influence of X on Y conditioned on Z [67]. In other words, TE has been extended to include the effect of the past of Z on the current state of the response Y and the past of X. This can be done by including the past of Z to the condition term of the conditional mutual information [19,67]:

$$PTE_{X\to Y|Z} = \mathrm{I}(Y_t; X_{t-1:t-\ell}|Y_{t-1:t-\ell}, Z_{t-1:t-\ell}) \tag{2–59}$$

In terms of entropy, PTE is defined as

$$PTE_{X\to Y|Z} = H(X_{t-1:t-\ell}, Y_{t-1:t-\ell}, Z_{t-1:t-\ell}) - H(Y_t, X_{t-1:t-\ell}, Y_{t-1:t-\ell}, Z_{t-1:t-\ell}) + H(Y_t, Y_{t-1:t-\ell}, Z_{t-1:t-\ell}) - H(Y_{t-1:t-\ell}, Z_{t-1:t-\ell}) \tag{2–60}$$

2.3.3. Directional partial mutual information (DPMI)

As we described earlier mutual information measures information shared between two time series. Now consider a third signal Z The partial mutual information $I(X,Y|Z)$ represent the part of mutual information $I(X,Y)$ that is not also shared with a third signal Z, given by Refs. [20,68]:

$$I(X;Y|Z) = H(X,Z) + H(Y,Z) - H(Z) - H(X,Y,Z) \tag{2–61}$$

PMI is symmetric, we extend this to give directional information by delaying one signal, hence calculating PMI between one signal and a lagged version of another signal. Directional partial mutual information, DPMI is determined by calculating partial mutual information for a range of lags and selecting then maximum value as the result. As only one signal is lagged, this introduces an asymmetry which allows access to the directional relationship between two signals.

2.3.4. Symbolic transfer entropy and partial symbolic transfer entropy

The symbolic transfer entropy (STE) and partial symbolic transfer entropy (PSTE) are defined similarly to TE and PTE, but the calculations use the ranks of the amplitudes rather than the amplitudes themselves [19,69]. Using ranks rather than amplitudes can assist in fine-tuning parameters, as the distribution of the data is known in advance. We implemented STE and PSTE using the Java Information Dynamics Toolkit [70].

2.3.5. Kullback-Leibler divergence

For densities P and Q, the Kullback-Leibler divergence is given by Ref. [71]:

$$K(P|Q) = \sum_i P_i \log\left(\frac{P_i}{Q_i}\right) \tag{2–62}$$

Rather than use pdfs, here we use the TFDs [6,49]:

$$K(C_x, C_y) = \sum_{n,f} C_x(n,f)\log\left(\frac{C_x(n,f)}{C_y(n,f)}\right) \tag{2–63}$$

where $C_x(n,f)$ and $C_{xy}(n,f)$ are the normalised auto- and cross-time-frequency distributions respectively, and can be calculated from the spectrogram $S_x(n,f)$ as:

$$C_x(n,f) = \frac{|S_x(n,f)|^2}{\sum_{n,f}|S_x(n,f)|^2} \tag{2–64}$$

$$C_{xy}(n,f) = \frac{|S_x(n,f)S_y^*(n,f)|}{\sum_{n,f}|S_x(n,f)S_y^*(n,f)|} \tag{2–65}$$

In this paper, we calculate the spectrogram using the short-term Fourier transform with a Hamming window.

2.3.6. Directional phase-locking value

Let $\phi_x(t)$ and $\phi_y(t)$ be the extracted phase from signals $x(t)$ and $y(t)$ respectively, via one of the techniques described above. Then, the (n, m) phase difference of the signals, where n and m are integers, can be defined as [72,73]:

$$\Delta\phi(t) = n\phi_x(t) - m\phi_y(t) \tag{2–66}$$

If the (n, m) phase difference of the signals remains bounded, then the signals are said to be n: m synchronised. In the most cases, only $m = n = 1$ is considered [40]. The mean phase coherence, also known as phase synchronisation index, R is given by Refs. [40,72,74,75]:

$$R = \langle e^{-i\Delta\phi(t)}\rangle = \sqrt{\langle\cos(\Delta\phi(t))\rangle^2 + \langle\sin(\Delta\phi(t))\rangle^2} \tag{2–67}$$

where the angle brackets represent an average over time. The mean phase coherence will be zero if the phases are not synchronised and will be one for a constant phase difference.

Mean phase coherence (or phase-locking value) quantifies the (symmetrical) phase relationship between two time series. Directional phase-locking value (dPLV) extends this to give directional information by delaying one signal, hence calculating mean phase coherence between $y(t)$ and a lagged version of time series $x(t - l)$. dPLV is determined by calculating these mean phase coherences for a range of lags and selecting then maximum value as the result. As only one signal is lagged, this introduces an asymmetry which allows access to the directional relationship between two signals.

$$\Delta\phi(t) = n\phi_x(t-l) - m\phi_y(t) \tag{2–68}$$

$$R(l) = \langle e^{-i\Delta\phi(t)}\rangle = \sqrt{\langle\cos(\Delta\phi(t))\rangle^2 + \langle\sin(\Delta\phi(t))\rangle^2} \tag{2–69}$$

$$dPLV = \max_{l=1,\ldots,L} R(l) \tag{2–70}$$

3. Methods

Here we focus on three simulated systems that mimic EEG in some way, where we have some knowledge or control of the level of nonlinearity, nonstationary and noise, and where we know the true connectivity patterns. First, we choose to study the Hénon map (system 1), as it is a well-understood nonlinear system that has been used extensively to examine synchronisation [3,15]. Second, we generate data from a seventh-order MVAR model with (system 2A) and without (system 2B) exogenous inputs. Finally, we generate simulated EEG consisting of a burst of alpha activity (system 3), to provide a more realistic assessment of the measures.

3.1. Hénon maps

The first simulation generated data from the system consists of three coupled Hénon maps with nonlinear couplings, $X_1 \rightarrow X_2 \rightarrow X_3$, defined by the following equations:

$$\begin{aligned} x_1(k+1) &= 1.4 + 0.3\,x_1(k-1) - x_1^2(k) \\ x_2(k+1) &= 1.4 + 0.3x_2(k-1) - [\mu\,x_1(k) + (1-\mu)x_2(k)]\,x_2(k) \\ x_3(k+1) &= 1.4 + 0.3x_3(k-1) - [\mu x_2(k) + (1-\mu)x_3(k)]x_3(k) \end{aligned} \tag{3-1}$$

Simulations used 2048 data points with fixed coupling strength μ, with the coupling strength varying across simulations from $\mu = 0$ (no coupling) to $\mu = 0.5$ (strong coupling).

Most measures have parameters that need to be selected, and that this can have a significant influence on their performance. Hence to optimize performance on system 1, and following the literature [76], we set the parameters as follows:

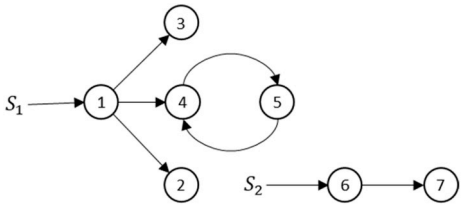

Fig. 2. The unweighted directed graph summarising the connections between signals in the MVAR model defined in equation(s) (3-2). $x_1(k) - x_7(k)$ denote the output signals of the model, $S_1(k)$ and $S_2(k)$ denote the exogenous inputs (EEG signals), and $e_1(k) - e_7(k)$ denote the white noise innovations of the MVAR

- For model-based measures, we set the model order $p = 2$.
- For frequency measures, we used the normalized range [0.4, 0.5] where the spectra of the signals show peaks, following [76].
- For measures that require a range of lags, e.g. PTE, we used the range 1–5 and the maximum value of the measure among the results was selected.

3.2. MVAR model

The second simulation is an MVAR model, inspired by the model used in Ref. [77], represented by the following set of linear difference equations with 7 nodes and exogenous sources $S_1(k)$ and $S_2(k)$ and illustrated in Fig. 2.

$$\begin{aligned} x_1(k) &= 0.95\sqrt{2}x_1(k-1) - 0.9025x_1(k-2) + e_1(k) + S_1(k) \\ x_2(k) &= 0.5x_1(k-1) + e_2(k) \\ x_3(k) &= -0.4x_1(k-3) + e_3(k) \\ x_4(k) &= -0.5x_1(k-1) + 0.25\sqrt{2}x_4(k-1) + 0.25\sqrt{2}x_5(k-1) + e_4(k) \\ x_5(k) &= -0.25\sqrt{2}x_4(k-1) + 0.25\sqrt{2}x_5(k-1) + e_5(k) \\ x_6(k) &= 0.95\sqrt{2}x_6(k-1) - 0.9025x_6(k-2) + e_6(k) + S_2(k) \\ x_7(k) &= -0.1x_6(k-2) + e_7(k) \end{aligned} \tag{3-2}$$

System 2A sets the exogenous inputs $S_1(k)$ and $S_2(k)$ to zero, whereas system 2B uses pre-processed EEG as the inputs. The EEG applied in the simulation was recorded at four locations (CP1, CP2, FC1, FC2) from a separate study during an eyes-closed resting or baseline task. The scalp recordings were pre-processed by filtering in the gamma frequency band (bandpass filter, 35–100 Hz), and 50001 data points (25 s sampled at 2 kHz) were used. All 12 different combinations of selecting $S_1(k)$ and $S_2(k)$ from these four channels were used in the simulations.

For model-based measures, the model order was optimized with multichannel Akaike Information Criterion (AIC) and set to $p = 3$ for the system 2A and set to $p = 5$ for the system 2B. For measures that optimise over a range of lags, the maximum lag was set by analogy to the optimized model order p. Frequency-based connectivity measures were calculated over the range of normalized frequencies [0, 0.4], consistent with other publications and also where the spectra of the signals is high [76].

3.3. Simulated EEG

3 channels of simulated EEG were generated, representing responses to repeated trials (Fig. 3). Each trial ran from −0.5 s to +1.0 s, and contained a noisy alpha burst with added pink noise at 0 dB. The alpha burst (a Hamming windowed 10 Hz sinusoid) ran from 300 ms to 700 ms with random timing jitter spread uniformly from −5 ms to +5 ms, and additional fixed delays of 20 ms in the second channel and 40 ms in the third channel. The amplitudes of the second and third

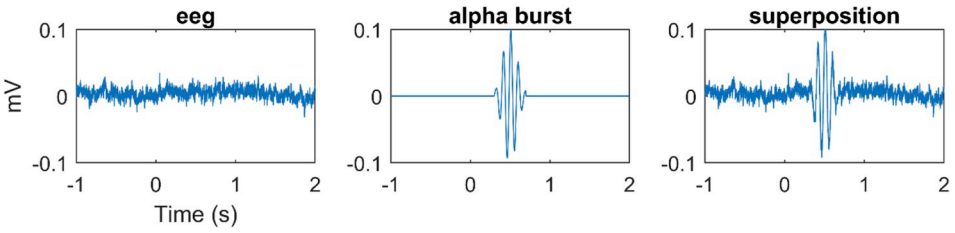

Fig. 3. Simulated eeg (left), alpha burst (middle) and superposition (right).

channels were set to 0.5 and 0.2 times the amplitude of the first channel respectively, modelling a delayed and reduced amplitude signal at two different locations to the source. The data were analysed for alpha connectivity using a sliding window of width 300 ms, sliding 50 ms between analyses. Frequency-based connectivity measures were estimated for the range of the alpha band (8–13 Hz). We averaged the measures over windows containing the alpha bursts (from 300 to 740 ms) where we expect measures to detect the direct causal connections $x_1 \rightarrow x_2$ and $x_1 \rightarrow x_3$. We also analysed the system over the time frame [0, 300 ms] where there is no causal connection between any pair of signals.

3.4. Statistical analyses

Note that direct comparisons between raw connectivity values for different measures is not appropriate. They are not measuring on the same scale, and significant variation in the raw values across measures can be seen. Hence to reliably compare different measures we need a statistical approach to identify when a connectivity value is significantly different from its background level.

To test the statistical significance of a connectivity value, surrogate data were generated to give data with the same statistical properties as the simulated data but without the dependencies between signals [78]. Several surrogate algorithms have been proposed [79,80], including the selected Iterative Amplitude Adjusted Fourier Transform surrogates [81]. These surrogate data have the same Fourier amplitudes as the original data but with random phases, and also have the same distribution of time-domain amplitudes. Since the conventional power spectral density is the modulus squared of the amplitude of the Fourier transform, the original data and its surrogate generated by this technique have the same power spectral densities. Any underlying interaction within the original data set is destroyed using phase randomisation. Hence any synchrony detected in surrogate signals will be due to chance. This type of surrogate, which maintains both the power spectrum and the amplitude distribution of the original data, is therefore well suited to analyse the nonlinearity and complexity of signals [82,83]. We note that calculations based on other surrogates will produce variation in the results, however our experience is that changing the surrogate algorithm does not have a significant effect on the results.

The connectivity measures were computed for the original signal and also for 100 surrogate realisations, and this was repeated for the 150 or 100 realisations of the simulated data. We represent these data overall with a connection matrix by testing whether the mean of the connectivity values from the original data is greater than the mean of the surrogates using a two-sample *t*-test at the 0.05 significance level. The decision of link or no-link is compared with the known truth for each pair of signals, and then drawn as a matrix, with colour indicating true positive, true negative, false positive or false negative. Additionally, we consider each realisation separately. The fifth largest of the one hundred surrogate measurements was selected as the threshold to give a 5% significance level. This allows a decision for each realisation by comparing the threshold from the surrogates to the measure computed on the original signal, so if the measure exceeds the threshold, then a link is indicated. Across the 150 or 100 realisations, this allows us to estimate the true positive rate (*TPR*, i.e. the proportion of actual links truly detected), false positive rate (*FPR*, i.e. the proportion of signals that are not linked that were falsely detected as linked), true negative rate (*TNR*, i.e. the proportion of signals that are not linked that were truly detected as not linked), and false negative rate (*FNR*, i.e. the proportion of actual links that were falsely detected as not linked). The *FPR* includes indirect causal connections, where a third signal mediates the interaction between the two signals under consideration.

4. Results

4.1. Results for system 1

Results for analysing the Hénon map data with the connectivity measures versus coupling strength μ are shown in Fig. 4, where the blue line shows the estimated connectivity strength and the red line shows the threshold for significance. When significance is achieved, the area between the two lines is filled in blue. The best result would show connectivity (filled blue area) only in the top central and central right squares. As can be seen from this figure, seven measures perform well in that the separation between the measure and its threshold increases with coupling strength: transfer entropy, partial Granger causality, conditional Granger causality, copula-Granger causality, multivariate Granger causality, spectral multivariate Granger causality and partial transfer entropy. These measures are able to detect all casual connections (true positives) but they also detect some connections that do not exist (false positives). Therefore we calculated the false positive rates (FPR), true positive rates (TPR), false negative rate (FNR) and true negative rate (TNR) for a deeper understanding, and the results are shown in Fig. 5. The measures in Fig. 5 have been sorted by informedness, i.e. the difference between the true positive rate and the false positive rate. Ideally we would have 100% TPR and 0% FPR, so the difference between these two can be used to rank measures. The partial transfer entropy and transfer entropy outperform other measures, achieving 100% and 80% detection of causal connections respectively, and 0% incorrect detection of an absence of a causal connection. Both measures obtain large positive values only for the two correct direct causal links, and this holds even for few data points and low coupling strengths μ. Extended Granger causality, copula-Granger causality, multivariate Granger causality in both the time and frequency domains, conditional Granger causality and partial Granger causality were able to detect all of the causal connections, but also incorrectly identified some absences of connections as connections. Extended directed coherence extended partial directed coherence and directed phase locking value performed little better than chance. Frequency domain conditional Granger causality, generalised partial directed coherence, partial directed coherence, directed transfer function, partial mutual information, generalised partial directed coherence and directed coherence displayed poor performance, incorrectly identifying more than 50% of the absences of connections as causal connections.

4.2. Results for system 2

For systems 2A and 2B, connection matrices are shown in Fig. 6 (a) and (b) respectively. The true/false positive/negative rates (expressed as percentages) for systems 2A and 2B are displayed in Fig. 7 (a) and (b) respectively. For both systems 2A and 2B, partial Granger causality,

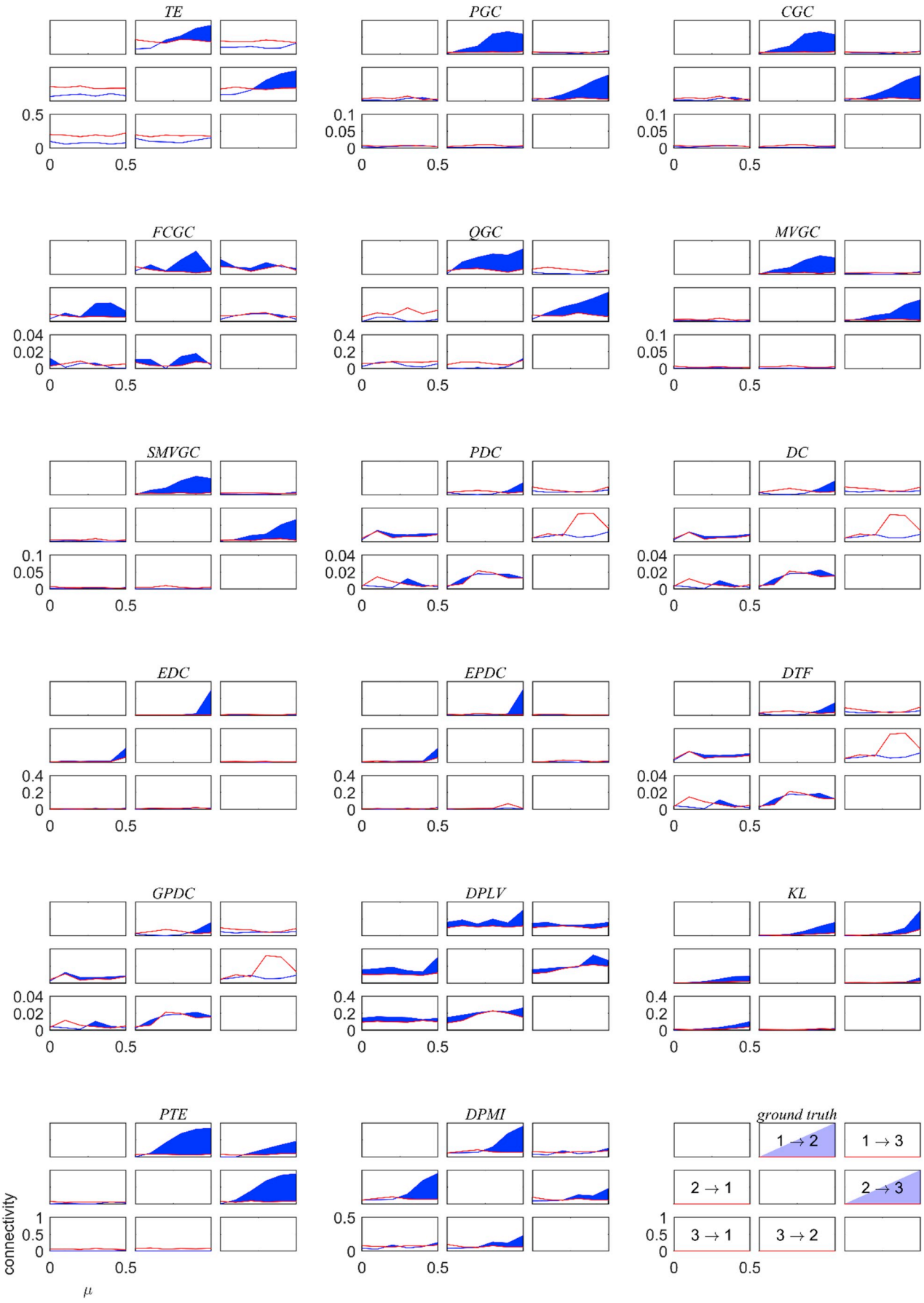

(caption on next page)

Fig. 4. Estimated connectivity strength (blue line) and threshold for significance (red line) for 17 connectivity measures versus coupling strength μ. When significance is achieved, the area between the two lines is filled in blue. The best result would show connectivity (filled blue area) only in the top central and central right squares, as suggested in the bottom right subplot. (For interpretation of the references to colour in this figure legend, the reader is referred to the Web version of this article.)

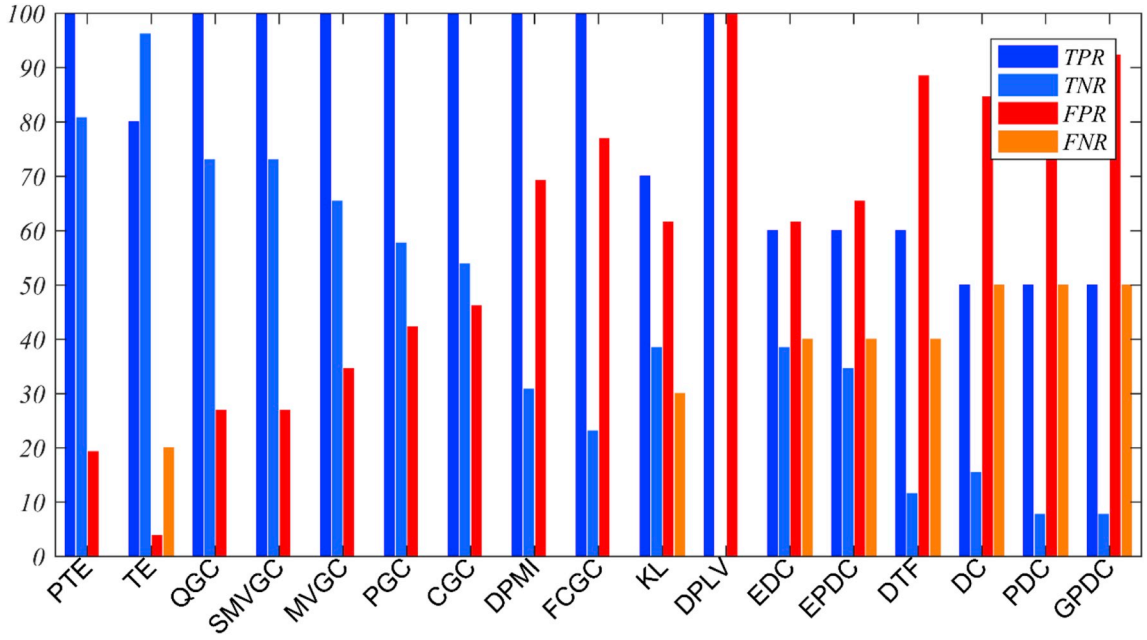

Fig. 5. The percentage of directed causal connections that were correctly identified (true positive rate, dark blue bars), the percentage of directed pairs that do not have a causal link that were correctly identified (true negative rate, light blue bars), the percentage of directed pairs that do not have a causal link that are identified incorrectly as a causal link (false positive rate, red bars), and the percentage of directed causal connections that are identified incorrectly as directed pairs that do not have a causal link (false negative rate, orange bars) for each effective connectivity measure analysing data from system 1. Measures are sorted by informedness. (For interpretation of the references to colour in this figure legend, the reader is referred to the Web version of this article.)

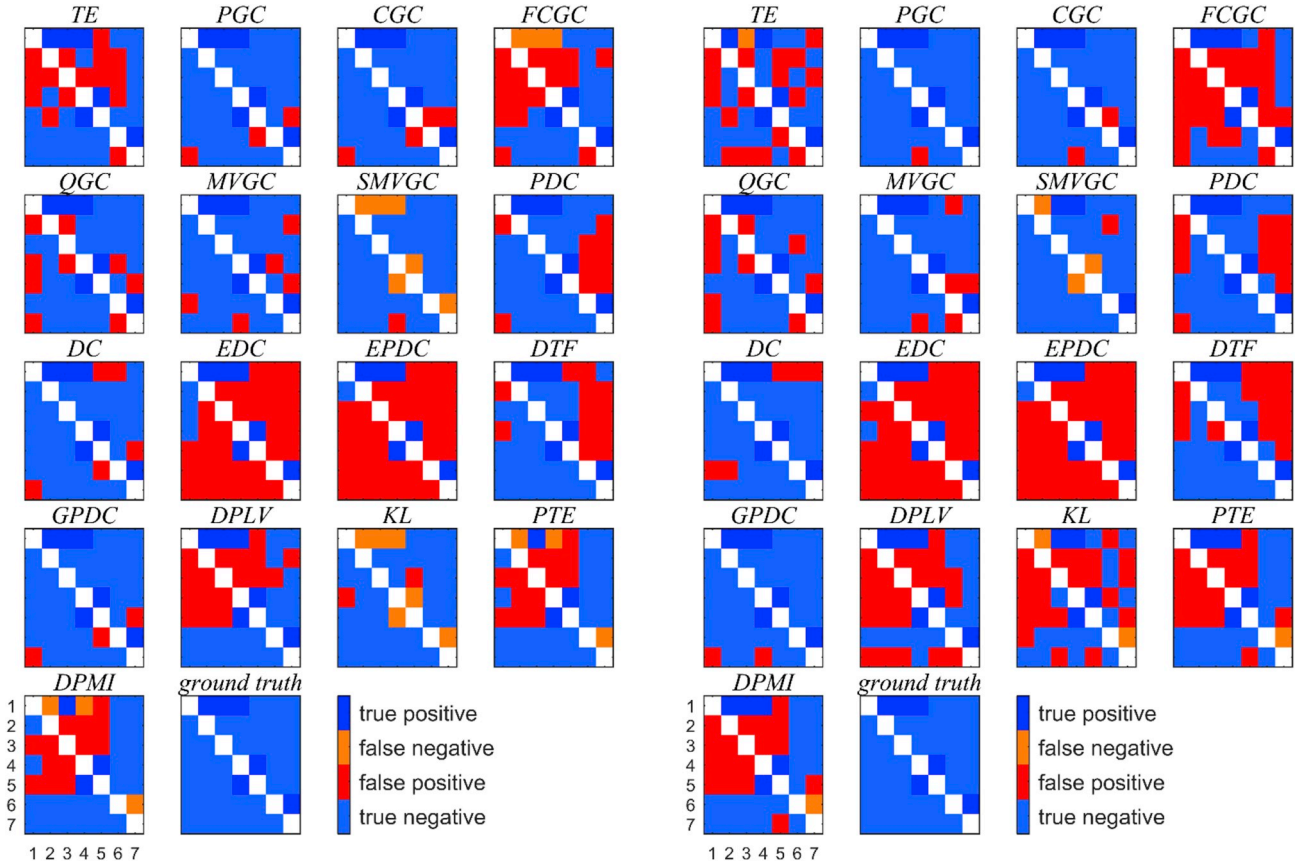

Fig. 6. Connection matrices for (a) system 2A and for (b) system 2B. Ground truth shows the true connectivity structure in the systems.

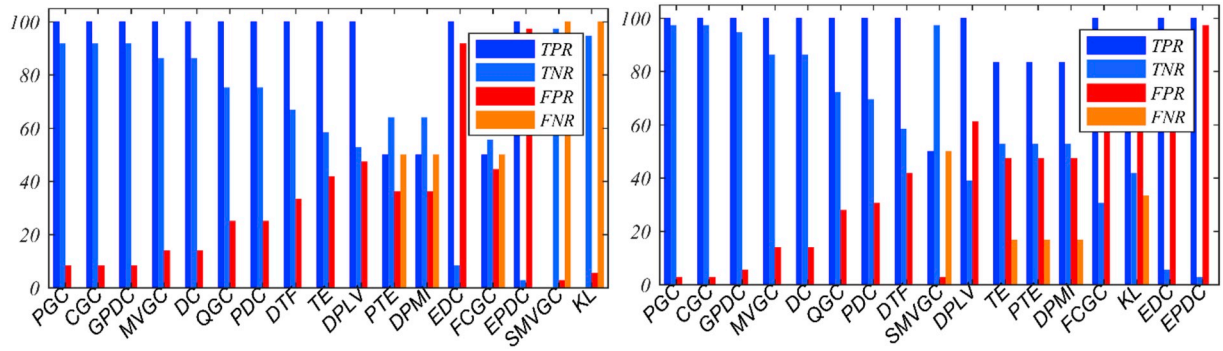

Fig. 7. The percentage of directed causal connections that were correctly identified (true positive rate, dark blue bars), the percentage of directed pairs that do not have a causal link that were correctly identified (true negative rate, light blue bars), the percentage of directed pairs that do not have a causal link that are identified incorrectly as a causal link (false positive rate, red bars), and the percentage of directed causal connections that are identified incorrectly as directed pairs that do not have a causal link (false negative rate, orange bars) for each effective connectivity measure analysing data from system 2A in (a) and for system 2B in (b). Measures are sorted by informedness. (For interpretation of the references to colour in this figure legend, the reader is referred to the Web version of this article.)

conditional Granger causality, and generalised partial coherence obtained the best results of all measures, with 100% true positive rate and less than 8% false positive rate. Multivariate Granger causality, copula-based Granger causality, partial directed coherence and directed coherence detected all causal connections correctly, but with larger false positive rates. The performance of directed transfer function has improved from its system 1 performance, however transfer entropy and partial transfer entropy showed worse performance. Unsatisfactory results were obtained in both system 2A and 2B for extended directed coherence, conditional frequency domain Granger causality, extended partial directed coherence, Kullback-Leibler divergence, and for multivariate frequency domain Granger causality in system 2A. Kullback-Leibler divergence and multivariate frequency domain Granger causality could not identify any of the six direct causal effects for system 2A.

4.3. Results for system 3

The results from system 3 for both time ranges are displayed in Fig. 8 and Fig. 9. Many measures correctly detect no connections for the time range from 0 to 300 ms as expected, namely transfer entropy, partial Granger causality, conditional Granger causality, Copula-based Granger causality, multivariate Granger causality, multivariate frequency domain Granger causality, partial transfer entropy and partial mutual information. During the alpha burst, directed coherence and

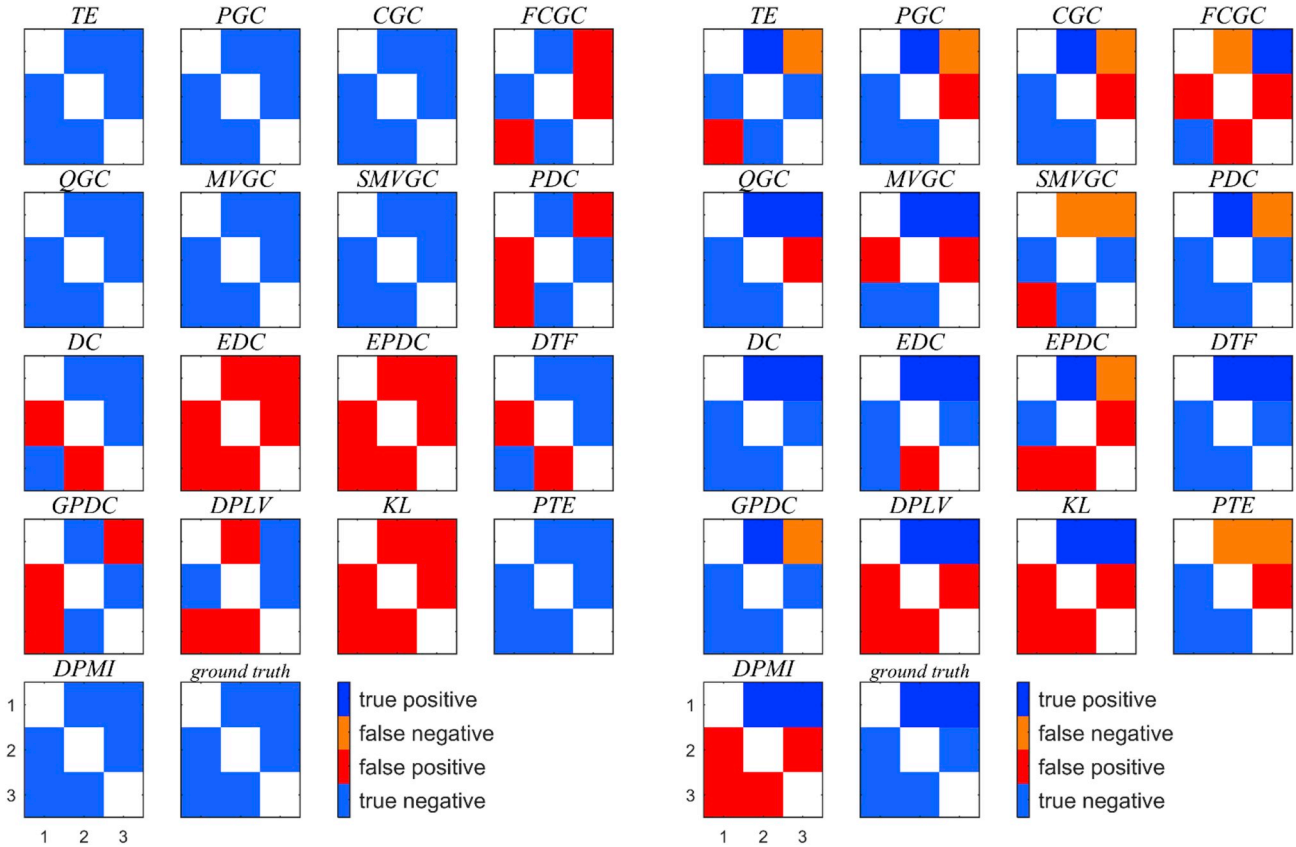

Fig. 8. Connection matrices for system 3 over the time ranges (a) 0–300 ms, where no causal connections exist, and (b) 300–740 ms, where direct causal connections do exist. Ground truth shows the true connectivity structure in the systems.

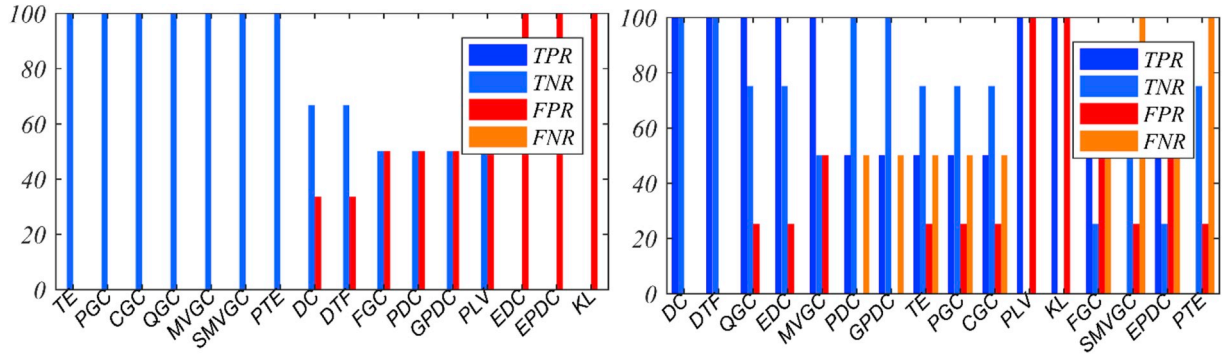

Fig. 9. The percentage of directed causal connections that were correctly identified (true positive rate, dark blue bars), the percentage of directed pairs that do not have a causal link that were correctly identified (true negative rate, light blue bars), the percentage of directed pairs that do not have a causal link that are identified incorrectly as a causal link (false positive rate, red bars), and the percentage of directed causal connections that are identified incorrectly as directed pairs that do not have a causal link (false negative rate, orange bars) for each effective connectivity measure analysing data from system 3, calculated over the time ranges (a) 0–300 ms, where no causal connections exist, and (b) 300–740 ms, where direct causal connections do exist. All measures are sorted by informedness. (For interpretation of the references to colour in this figure legend, the reader is referred to the Web version of this article.)

Table 1
The time (seconds) required to estimate each measure for three sizes of data: few data ($N_{samples}$ = 300) and few channels ($N_{channels}$ = 3), many data ($N_{samples}$ = 50001) and few channels ($N_{channels}$ = 3), and few data ($N_{samples}$ = 300) and many channels ($N_{channels}$ = 60).

	Time (s)		
Measure	$N_{samples}$ = 300 $N_{channels}$ = 3	$N_{samples}$ = 50001 $N_{channels}$ = 3	$N_{samples}$ = 300 $N_{channels}$ = 60 model order = max lag = 5
PGC	0.024	0.447	771.783
FGC	0.031	0.031	10.918
DC	0.188	0.404	19.406
DTF	0.188	0.404	19.406
PDC	0.188	0.404	19.406
EPDC	0.188	0.404	19.406
EDC	0.188	0.404	19.406
GPDC	0.188	0.404	19.406
QGC	0.041	14.367	3.974
MVGC	0.025	0.029	21.562
TE	0.013	0.017	0.960
PMI	0.104	13.828	2864
PTI	0.103	9.322	2718
CGC	0.010	0.100	6.114
SMVGC	0.030	0.039	390.264
KL	0.046	0.066	6.133

directed transfer function correctly found all connections and no others, Copula-based Granger causality and extended directed coherence correctly found all connections but incorrectly identified a third connection, and partial directed coherence and generalized partial directed coherence found one of the two connections correctly.

4.4. Execution time

It is important to note that different measures require different calculations that take different amounts of time. In particular, partial and conditional measures would reasonably be expected to require longer execution times. Table 1 lists the execution times for the 17 effective connectivity measures under three conditions: few data and few channels, many data and few channels, and many data and many channels. Computations for this table were performed in Matlab R2017b using 128 channels of real EEG on a Windows10 PC with 16 GB of RAM and an i7-7700 CPU running at 3.6 GHz.

It is preferable, in general, for a measure to scale slowly with the number of samples and the number of channels, though in some situations this may not be necessary. Overall, transfer entropy is the fastest measure, followed by frequency-domain Granger causality, multivariate Granger causality, conditional Granger causality and Kullback-Leibler divergence, all of which scale less well with the number of channels. Execution time increases significantly for partial transfer entropy and partial mutual information for with both the number of channels and the number of data. Partial Granger causality and frequency domain multivariate Granger causality scale poorly with the number of channels, and copula Granger causality scales poorly with the number of data.

5. Discussion and conclusion

Previous studies of effective connectivity measures have concentrated on a few measures. Some studies focused on model-based measures, others have considered information theoretic measures or phase-based measures, while some studies have compared effective and functional connectivity measures. There is no thorough comparison of many effective connectivity measures from different families on simulated data. Here we include most of the well-known effective connectivity measures from different families, including model-based measures, information theoretic measures, and directional phase locking value. Because of the differences in approach, it is not straightforward to compare our results with previous studies, so we comment only where a useful comparison is possible, typically a paper that compares more than one effective connectivity measure and where there is a known or believed outcome that can be used to compare the performance of these measures.

Wu et al. [84] compared six multivariate causality measures, three of which are included in our study (multivariate Granger causality, directed transfer function, and partial directed coherence). When tested on simulated MVAR data, their conclusion was that Granger causality outperformed the two other measures, consistent with our finding. Additionally, both [84] and this study found Granger causality outperformed all other measures from the directed coherence family.

Papana et al. [76] assessed the performance of the six directed causality measures: conditional Granger causality, partial Granger causality, partial directed coherence, partial transfer entropy, partial symbolic transfer entropy and partial mutual information on mixed embedding. All these measures were included in our studies except partial mutual information, as its execution time is prohibitively large. The datasets used were four linear MVAR models, including one with latent and exogenous inputs, and three nonlinear models (including one nearly identical to the Hénon map system studied here). They found that conditional Granger causality, partial Granger causality and partial directed coherence performed better than other measures for the linear systems, with partial Granger causality best when latent and exogenous

Table 2
TPR, TNR, FPR and FNR for all measures and all systems, and an overall measure of performance. Optimum rates are coloured green, fading to white at performance equal to chance, strengthening to red as performance approaches all decisions incorrect.

	measure	TPR					TNR					FPR					FNR				
overall		S1	S2A	S2B	S3n	S3	S1	S2A	S2B	S3n	S3	S1	S2A	S2B	S3n	S3	S1	S2A	S2B	S3n	S3
55	TE	80	100	83		50	96	58	53	100	75	4	42	47	0	25	20	0	17		50
71	PGC	100	100	100		50	58	92	97	100	75	42	8	3	0	25	0	0	0		50
70	CGC	100	100	100		50	54	92	94	100	75	46	8	6	0	25	0	0	0		50
8	FCGC	100	50	100		50	23	56	31	50	25	77	44	69	50	75	0	50	0		50
77	QGC	100	100	100		100	73	75	72	100	75	27	25	28	0	25	0	0	0		0
75	MVGC	100	100	100		100	65	86	86	100	50	35	14	14	0	50	0	0	0		0
32	SMVGC	100	0	50		0	73	97	97	100	75	27	3	3	0	25	0	100	50		100
34	PDC	50	100	100		50	8	75	69	50	100	92	25	31	50	0	50	0	0		50
57	DC	50	100	100		100	15	86	86	67	100	85	14	14	33	0	50	0	0		0
8	EDC	60	100	100		100	39	8	6	0	75	62	92	94	100	25	40	0	0		0
-17	EPDC	60	100	100		50	35	3	3	0	25	65	97	97	100	75	40	0	0		50
47	DTF	60	100	100		100	12	67	58	67	100	89	33	42	33	0	40	0	0		0
43	GPDC	50	100	100		50	8	92	94	50	100	92	8	6	50	0	50	0	0		50
20	DPLV	100	100	100		100	0	53	39	50	0	100	47	61	50	100	0	0	0		0
-9	KL	70	0	67		100	39	94	42	0	0	62	6	58	100	100	30	100	33		0
35	PTE	100	50	83		0	81	64	53	100	75	19	36	47	0	25	0	50	17		100
29	DPMI	100	50	83		100	31	64	53	100	0	69	36	47	0	100	0	50	17		0

inputs were present. The non-directional measure partial mutual information on mixed embedding outperformed all others for the nonlinear systems. Similarly, our studies showed that copula Granger causality, multivariate Granger causality, partial Granger causality and conditional Granger causality performed best overall for MVAR systems, whereas transfer entropy should be preferred for nonlinear systems. Consistent with [76], Granger causality measures perform best for linear models, and an information theoretic measure performs best for nonlinear models.

Guo et al. [32] introduced partial Granger causality and tested partial Granger causality and conditional Granger causality with data from an MVAR model with exogenous and latent inputs. Their results demonstrated that partial Granger causality can reliably detect effective connections between signals in the presence of exogenous inputs, whereas conditional Granger causality frequently fails. In contrast, our results show little difference between partial Granger causality and conditional Granger causality, though the largest difference does occur with System 2B, which is an MVAR model with exogenous inputs.

Papana et al. [85] compared two effective connectivity measures, the nonlinear measure partial transfer entropy and the linear measure partial directed coherence, on one linear MVAR model and two nonlinear models (again, one being a similar Hénon map model). Their results showed that for the linear model, partial transfer entropy and partial directed coherence performed equally well, whereas for the nonlinear models partial transfer entropy performed better than partial directed coherence. A similar study [7] compared six connectivity measures: three functional connectivity measures (cross correlation, coherence and phase synchronisation index) and three directional measures (transfer entropy, directed transfer function and partial directed coherence). They used simulated data generated from an MVAR model with two exogenous inputs (similar to the system 2B studied in this theses). They concluded that directed transfer function and partial directed coherence performed better than other measures. With one exception, these results are consistent with our findings, and consistent with the view that the best linear measures outperform the best nonlinear measures on linear data, but the best nonlinear measures outperform the best linear measures on data drawn from nonlinear models. The exception here is that [7] found that linear and nonlinear measures performed equally on linear data. This may be due to their use of a small three-node MVAR model with strong coupling, making the task of identifying connections relatively easy. Faes et al. [45] introduced two extended causality measures of directed coherence and partial directed coherence, namely extended directed coherence and extended partial directed coherence. They claim that traditional directed coherence and partial directed coherence may produce misleading connectivity patterns when there are instantaneous links between signals. Their results show better performance using the extended measures. Our results for System 1 are consistent: where there are instantaneous links between signals, the extended measures outperform the original measures. However, we found that for all other systems, where there are no instantaneous links, the extended measures performance is worse than the original measures. Faes et al. [38] also note that EDC and EPDC rely on additional assumptions, either prior knowledge of the directionality of connections or regarding the non-Gaussianity of innovations to the model. Exploratory studies in EEG may not be able to rely on either of these assumptions. Given no other studies on the extended measures, we do not recommend their use unless the studied system is known to have instantaneous links.

Smit et al. [86] compared two effective connectivity measures, transfer entropy and directed transfer function, in high density resting state EEG data in eyes open and eyes close. They found that the differences between the eyes closed and eyes open condition identified by transfer entropy better matched the expectations from the literature than the differences found by DTF. Our results also found that transfer entropy outperformed DTF, and particularly when the data were not drawn from an MVAR model.

C Yang in Ref. [87] compared 11 effective connectivity measure from three different group of measures from the Granger causality, transfer entropy and directed coherence families. They tested measures on simulated data generated from linear and nonlinear MVAR models, a physiology-based model, and real signals. All their considered measures are included in this study, but the models are different Their results show that conditional Granger causality, partial directed coherence and partial transfer entropy (called conditional transfer entropy in Ref. [87]) performed best in their respective families. No comparison was made across families. Consistent with their results, our results also show that conditional Granger causality performed best in its family. However, our results only showed partial transfer entropy as best in family

for S1 (data not drawn from an MVAR model), and partial directed coherence was never best in family.

In summary, we considered 17 of the best-known connectivity measures and studied their performance for different sets of simulated time series (S1: non-linear coupled Hénon maps, S2a and S2b: MVAR model, and S3: simulated EEG). Table 2 shows the TPR, TNR, FPR and FNR for all measures and all systems, and an overall measure of performance. Optimum rates are coloured green, fading to white at performance equal to chance, strengthening to red as performance approaches all decisions incorrect. Copula Granger causality, multivariate Granger causality, partial Granger causality and conditional Granger causality performed best overall, with good performance in almost every situation. Partial Granger causality was therefore the best of the "partial" measures (partial Granger causality, partial directed coherence, partial transfer entropy), consistent with the findings in Ref. [76].

Partial transfer entropy and transfer entropy performed very well when the data were not generated from an MVAR system but did not give as good results when the data were drawn from an MVAR model. Directed coherence and directed transfer function performed poorly on system 1, where the data are not drawn from an MVAR system and do not have energy concentrated in a specific frequency range. For system 2, when the data are MVAR, and system 3, where the data are focussed in a specific frequency band, they performed well. The worst performance was obtained by extended directed coherence and extended partial directed coherence, where almost all pairs of signals are deemed to have a connection. The addition of exogenous EEG inputs did not have any significant effect on the TPR of any connectivity measure except TE, whose performance degraded. However, several measures showed decreases in TNR, indicating that the presence of exogenous inputs results in an increase in the identification of false connections.

Our results suggest that there is not one measure that is consistently superior to all other measures, and that performance is critically dependent on the genesis of the data under analysis.

Overall, the measure with the best performance in a variety of situations and a low computational cost is conditional Granger causality. Partial Granger causality and multivariate Granger causality can also be used as reliable measures, but their computational cost rises rapidly with the number of channels. Similarly, copula Granger causality can also be used reliably, but its computational cost rises rapidly with the number of data. This may not be an issue if the data under analysis is epoched to handle non-stationarity.

We note again that all measures have parameters that need to be set, such as model order or number of bins etc. Improvements in selecting values for these parameters could have a substantial effect on comparisons of measures. Another area of possible improvement is in the generation of simulated data that more reliably reproduces EEG. The difficulty is in the validation of such models of EEG.

For EEG data, where the genesis of the data is unknowable, we recommend that using more than one measure is wise. Including a measure from each family, such as copula Granger causality or conditional Granger causality from the Granger causality family, along with transfer entropy as an information theoretic measure, and directed coherence from the coherence family, would be an appropriate choice.

References

[1] C.W.J. Granger, Testing for causality: a personal viewpoint, J. Econ. Dyn. Control 2 (1980) 329–352.
[2] B. Schelter, et al., Testing for directed influences among neural signals using partial directed coherence, J. Neurosci. Methods 152 (1) (2006) 210–219.
[3] J.-W. Xu, et al., A new nonlinear similarity measure for multichannel signals, Neural Network. 21 (2) (2008) 222–231.
[4] H.G. Schuster, Reviews of Nonlinear Dynamics and Complexity, Wiley, 2010.
[5] A.S. Janani, et al., Improved artefact removal from EEG using Canonical Correlation Analysis and spectral slope, J. Neurosci. Methods 298 (2018) 1–15.
[6] J. Dauwels, et al., A comparative study of synchrony measures for the early diagnosis of Alzheimer's disease based on EEG, Neuroimage 49 (1) (2010) 668–693.
[7] M.J. Silfverhuth, et al., Experimental comparison of connectivity measures with simulated EEG signals, Med. Biol. Eng. Comput. 50 (7) (2012) 683–688.
[8] H.E. Wang, et al., A systematic framework for functional connectivity measures, Front. Neurosci. 8 (2014) 405.
[9] H. Bakhshayesh, et al., Detecting synchrony in EEG: a comparative study of functional connectivity measures, Comput. Biol. Med. 105 (February 2019) 1–15 https://doi.org/10.1016/j.compbiomed.2018.12.005.
[10] J. Bhattacharya, E. Pereda, H. Petsche, Effective detection of coupling in short and noisy bivariate data, IEEE Trans. Syst. Man Cybern. B Cybern. 33 (1) (2003) 85–95.
[11] R.Q. Quiroga, J. Arnhold, P. Grassberger, Learning driver-response relationships from synchronization patterns, Phys. Rev. 61 (5) (2000) 5142.
[12] R.Q. Quiroga, et al., Reply to "Comment on 'Performance of different synchronization measures in real data: a case study on electroencephalographic signals'", Phys. Rev. 67 (6) (2003) 063902.
[13] A. Gunduz, J.C. Principe, Correntropy as a novel measure for nonlinearity tests, Signal Process. 89 (1) (2009) 14–23.
[14] M.C. Romano, et al., Estimation of the direction of the coupling by conditional probabilities of recurrence, Phys. Rev. 76 (3) (2007) 036211.
[15] S.J. Schiff, et al., Detecting dynamical interdependence and generalized synchrony through mutual prediction in a neural ensemble, Phys. Rev. 54 (6) (1996) 6708.
[16] M. Kamiński, et al., Evaluating causal relations in neural systems: granger causality, directed transfer function and statistical assessment of significance, Biol. Cybern. 85 (2) (2001) 145–157.
[17] L. Astolfi, et al., Assessing cortical functional connectivity by partial directed coherence: simulations and application to real data, IEEE Trans. Biomed. Eng. 53 (9) (2006) 1802–1812.
[18] T. Schreiber, Measuring information transfer, Phys. Rev. Lett. 85 (2) (2000) 461–464.
[19] D. Kugiumtzis, Partial Transfer Entropy on Rank Vectors, (2013) arXiv preprint arXiv:1303.6454.
[20] S. Frenzel, B. Pompe, Partial mutual information for coupling analysis of multivariate time series, Phys. Rev. Lett. 99 (20) (2007) 204101.
[21] H. Bakhshayesh, et al., Towards detecting connectivity in eeg: a comparative study of parameters of effective connectivity measures on simulated data, IEEE-EMBS Conference on Biomedical Engineering and Sciences (IECBES). 2018, IEEE, 2018.
[22] L. Baccala, et al., Studying the interaction between brain structures via directed coherence and Granger causality, Appl. Signal Process. 5 (1) (1998) 40.
[23] B. Gourévitch, R. Le Bouquin-Jeannes, G. Faucon, Linear and nonlinear causality between signals: methods, examples and neurophysiological applications, Biol. Cybern. 95 (4) (2006) 349–369.
[24] C.W. Granger, Investigating causal relations by econometric models and cross-spectral methods, Econometrica: J. Econom. Soc. (1969) 424–438.
[25] C.W. Granger, Testing for causality: a personal viewpoint, J. Econ. Dyn. Control 2 (1980) 329–352.
[26] J. Geweke, Measurement of linear dependence and feedback between multiple time series, J. Am. Stat. Assoc. 77 (378) (1982) 304–313.
[27] P.A. Stokes, P.L. Purdon, A study of problems encountered in Granger causality analysis from a neuroscience perspective, Proc. Natl. Acad. Sci. Unit. States Am. 114 (34) (2017) E7063–E7072.
[28] L. Barnett, A.K. Seth, The MVGC multivariate Granger causality toolbox: a new approach to Granger-causal inference, J. Neurosci. Methods 223 (0) (2014) 50–68.
[29] S. Malekpour, W.A. Sethares, Conditional Granger causality and partitioned Granger causality: differences and similarities, Biol. Cybern. 109 (6) (2015) 627–637.
[30] J.F. Geweke, Measures of conditional linear dependence and feedback between time series, J. Am. Stat. Assoc. 79 (388) (1984) 907–915.
[31] B. Schelter, M. Winterhalder, J. Timmer, Handbook of Time Series Analysis: Recent Theoretical Developments and Applications, John Wiley & Sons, 2006.
[32] S. Guo, et al., Partial Granger causality—eliminating exogenous inputs and latent variables, J. Neurosci. Methods 172 (1) (2008) 79–93.
[33] M.T. Bahadori, Y. Liu, An examination of practical granger causality inference, Proceedings of the 2013 SIAM International Conference on Data Mining, SIAM, 2013.
[34] Y. Liu, T. Bahadori, H. Li, Sparse-gev: Sparse Latent Space Model for Multivariate Extreme Value Time Serie Modeling, (2012) arXiv preprint arXiv:1206.4685.
[35] L.A. Baccalá, K. Sameshima, Partial directed coherence: a new concept in neural structure determination, Biol. Cybern. 84 (6) (2001) 463–474.
[36] G.M. Jenkins, D.G. Watts, Spectral Analysis and its Applications, Holden-Day, 1969.
[37] G.T. Wilson, The factorization of matricial spectral densities, SIAM J. Appl. Math. 23 (4) (1972) 420–426.
[38] L. Faes, et al., A framework for assessing frequency domain causality in physiological time series with instantaneous effects, Phil. Trans. Math. Phys. Eng. Sci. 371 (2013) 20110618 1997.
[39] F.T. Sun, L.M. Miller, M. D'esposito, Measuring interregional functional connectivity using coherence and partial coherence analyses of fMRI data, Neuroimage 21 (2) (2004) 647–658.
[40] R.Q. Quiroga, Bivariable and Multivariable Analysis of EEG Signals, (2009).
[41] M. Kaminski, K.J. Blinowska, A new method of the description of the information flow in the brain structures, Biol. Cybern. 65 (3) (1991) 203–210.
[42] M. Kaminski, H. Liang, Causal influence: advances in neurosignal analysis, Crit. Rev. Biomed. Eng. 33 (4) (2005).
[43] L.A. Baccalá, K. Sameshima, D. Takahashi, Generalized partial directed coherence, Digital Signal Processing, 2007 15th International Conference on, IEEE, 2007.
[44] A. Korzeniewska, et al., Determination of information flow direction among brain structures by a modified directed transfer function (dDTF) method, J. Neurosci. Methods 125 (1–2) (2003) 195–207.

[45] L. Faes, G. Nollo, Multivariate frequency domain analysis of causal interactions in physiological time series, Biomedical Engineering, Trends in Electronics, Communications and Software, InTech, 2011.
[46] L. Faes, G. Nollo, Extended causal modeling to assess Partial Directed Coherence in multiple time series with significant instantaneous interactions, Biol. Cybern. 103 (5) (2010) 387–400.
[47] C. Krier, et al., Feature scoring by mutual information for classification of mass spectra, Appl. Artif. Intell. 10 (2006) 557–564.
[48] S. Aviyente, Information theoretic measures for quantifying the integration of neural activity, Information Theory and Applications Workshop, 2007, IEEE, 2007.
[49] M.S. Khalid, et al., Kullback-Leiber divergence measure in correlation of gray-scale objects, Proc. 2nd IntŠl Conf. On Innovations in Information Technology (IIT05), 2005.
[50] J.T. Lizier, Measuring the dynamics of information processing on a local scale in time and space, Directed Information Measures in Neuroscience, Springer, 2014, pp. 161–193.
[51] A. Lancichinetti, S. Fortunato, J. Kertesz, Detecting the overlapping and hierarchical community structure in complex networks, New J. Phys. 11 (3) (2009) 033015.
[52] L. Ana, A.K. Jain, Robust data clustering, Computer Vision and Pattern Recognition, 2003. Proceedings. 2003 IEEE Computer Society Conference on, IEEE, 2003.
[53] A.F. McDaid, D. Greene, N. Hurley, Normalized Mutual Information to Evaluate Overlapping Community Finding Algorithms, (2011) arXiv preprint arXiv:1110.2515.
[54] R. Vicente, et al., Transfer entropy—a model-free measure of effective connectivity for the neurosciences, J. Comput. Neurosci. 30 (1) (2011) 45–67.
[55] P.-O. Amblard, O.J. Michel, On directed information theory and Granger causality graphs, J. Comput. Neurosci. 30 (1) (2011) 7–16.
[56] K. Hlaváčková-Schindler, et al., Causality detection based on information-theoretic approaches in time series analysis, Phys. Rep. 441 (1) (2007) 1–46.
[57] M. Vejmelka, M. Paluš, Inferring the directionality of coupling with conditional mutual information, Phys. Rev. 77 (2) (2008) 026214.
[58] R. Vicente, M. Wibral, Efficient estimation of information transfer, Directed Information Measures in Neuroscience, Springer, 2014, pp. 37–58.
[59] M. Wibral, R. Vicente, J.T. Lizier, Directed Information Measures in Neuroscience, Springer, 2014.
[60] M. Wibral, et al., Transfer entropy in magnetoencephalographic data: quantifying information flow in cortical and cerebellar networks, Prog. Biophys. Mol. Biol. 105 (1–2) (2011) 80–97.
[61] J.A.V. Butler, D. Noble, Progress in Biophysics and Molecular Biology, Elsevier, 2014.
[62] A. Montalto, L. Faes, D. Marinazzo, MuTE: a MATLAB toolbox to compare established and novel estimators of the multivariate transfer entropy, PLoS One 9 (10) (2014) e109462.
[63] D. Marinazzo, M. Pellicoro, S. Stramaglia, Causal information approach to partial conditioning in multivariate data sets, Comput. Math. Methods Med. 2012 (2012) 3036018 pages.
[64] I. Vlachos, D. Kugiumtzis, Nonuniform state-space reconstruction and coupling detection, Phys. Rev. 82 (1) (2010) 016207.
[65] M. Paluš, V. Albrecht, I. Dvořák, Information theoretic test for nonlinearity in time series, Phys. Lett. 175 (3–4) (1993) 203–209.
[66] K. Rutanen, TIM 1.2.0, (2011) [cited 2019 21/05/2019]; Available from: https://www.cs.tut.fi/~timhome/tim/tim.htm.
[67] A. Papana, D. Kugiumtzis, C. Kyrtsou, A nonparametric causality test: detection of direct causal effects in multivariate systems using corrected partial transfer entropy, Topics in Nonparametric Statistics, Springer, 2014, pp. 197–206.
[68] I. Luna, S. Soares, R. Ballini, Partial mutual information criterion for modelling time series via neural networks, Proc. Of the 11th Information Processing and Management of Uncertainty International Conference, 2006.
[69] M. Staniek, K. Lehnertz, Symbolic transfer entropy, Phys. Rev. Lett. 100 (15) (2008) 158101.
[70] J.T. Lizier, JIDT: an information-theoretic toolkit for studying the dynamics of complex systems, Front. Robot. Artif. Intell. 1 (2014) 11.
[71] S. Kullback, R.A. Leibler, Ann. Math. Stat. 22 (1951) 79–86.
[72] A. Pikovsky, M. Rosenblum, J. Kurths, Synchronization: a Universal Concept in Nonlinear Sciences vol. 12, Cambridge university press, 2003.
[73] P. Tass, et al., Detection of n: m phase locking from noisy data: application to magnetoencephalography, Phys. Rev. Lett. 81 (15) (1998) 3291.
[74] F. Mormann, et al., Mean phase coherence as a measure for phase synchronization and its application to the EEG of epilepsy patients, Phys. Nonlinear Phenom. 144 (3) (2000) 358–369.
[75] M. Rosenblum, et al., Phase synchronization: from theory to data analysis, Handb. Biol. Phys. 4 (279–321) (2001) 93–94.
[76] A. Papana, et al., Simulation study of direct causality measures in multivariate time series, Entropy 15 (7) (2013) 2635–2661.
[77] L.A. Baccalá, K. Sameshima, Overcoming the limitations of correlation analysis for many simultaneously processed neural structures, Prog. Brain Res. 130 (2001) 33–47.
[78] J. Theiler, D. Prichard, Constrained-realization Monte-Carlo method for hypothesis testing, Phys. Nonlinear Phenom. 94 (4) (1996) 221–235.
[79] L. Faes, A. Porta, G. Nollo, Testing frequency-domain causality in multivariate time series, IEEE Trans. Biomed. Eng. 57 (8) (2010) 1897–1906.
[80] T. Schreiber, A. Schmitz, Surrogate time series, Phys. Nonlinear Phenom. 142 (3–4) (2000) 346–382.
[81] T. Schreiber, A. Schmitz, Improved surrogate data for nonlinearity tests, Phys. Rev. Lett. 77 (4) (1996) 635.
[82] A. Porta, et al., Complexity and nonlinearity in short-term heart period variability: comparison of methods based on local nonlinear prediction, IEEE (Inst. Electr. Electron. Eng.) Trans. Biomed. Eng. 54 (1) (2007) 94–106.
[83] R. Benitez, et al., Characterization of the nonlinear content of the heart rate dynamics during myocardial ischemia, Med. Eng. Phys. 31 (6) (2009) 660–667.
[84] M.-H. Wu, R.E. Frye, G. Zouridakis, A comparison of multivariate causality based measures of effective connectivity, Comput. Biol. Med. 41 (12) (2011) 1132–1141.
[85] A. Papana, D. Kugiumtzis, P.G. Larsson, Detection of direct causal effects and application to epileptic electroencephalogram analysis, Int. J. Bifurc. Chaos 22 (09) (2012) 1250222.
[86] D.J. Smit, et al., Heritability of “small-world” networks in the brain: a graph theoretical analysis of resting-state EEG functional connectivity, Hum. Brain Mapp. 29 (12) (2008) 1368–1378.
[87] C. Yang, Contribution à l'analyse de connectivité effective en épilepsie, PhD report, 1 Université Rennes, 2012.